https://doi.org/10.1038/s41586-022-05679-w

The carbon sink of secondary and degraded humid tropical forests

Authors

Viola H. A. Heinrich[1,2*], Christelle Vancutsem[3,4], Ricardo Dalagnol[5,6,7], Thais M. Rosan[2], Dominic Fawcett[2], Celso H. L. Silva-Junior[6,7,8], Henrique L. G. Cassol[5,9], Frédéric Achard[10], Tommaso Jucker[11], Carlos A. Silva[12], Jo House[1], Stephen Sitch[2], Tristram C. Hales[13], Luiz E. O. C. Aragão[2,5]

Affiliations and Addresses

[1]School of Geography, University of Bristol, Bristol, UK.

[2]Faculty of Environment, Science and Economy, University of Exeter, Exeter, UK.

[3]FINCONs group, Milan, Italy

[4]Center for International Forestry Research (CIFOR), Bogor, Indonesia

[5]Earth Observation and Geoinformatics Division, National Institute for Space Research (INPE), São José dos Campos, Brazil.

[6]Institute of the Environment and Sustainability, University of California, Los Angeles - UCLA, CA 90095 USA

[7]NASA-Jet Propulsion Laboratory, California Institute of Technology, Pasadena, CA 91109, USA

[8]Programa de Pós-graduação em Biodiversidade e Conservação, Universidade Federal do Maranhão - UFMA, São Luís, MA, Brazil.

[9]School of Geosciences, University of Edinburgh, Edinburgh, UK.

[10] European Commission, Joint Research Centre, Ispra, Italy.

[11]School of Biological Sciences, University of Bristol, Bristol UK.

[12]Forest Biometrics and Remote Sensing Laboratory (Silva Lab), School of Forest, Fisheries, and Geomatics Sciences, University of Florida, Gainesville, FL, USA.

[13]Sustainable Places Research Institute, Cardiff University, Cardiff, UK.

Corresponding author Contact:

*Email: viola.heinrich@bristol.ac.uk

Summary Paragraph

The globally important carbon sink of intact, old-growth tropical humid forests is declining because of climate change, deforestation and degradation from fire and logging[1–3]. Recovering tropical secondary and degraded forests now cover about 10% of the tropical forest area[4], but how much carbon they accumulate remains uncertain. Here we quantify the aboveground carbon sink of recovering forests across three major continuous tropical humid regions: the Amazon, Borneo and Central Africa[5,6]. Based on satellite data products[4,7], our analysis encompasses the heterogenous spatial and temporal patterns of growth in degraded and secondary forests, influenced by key environmental and anthropogenic drivers. In the first twenty years of recovery, regrowth rates in Borneo were up to 45% and 58% higher than in Central Africa and the Amazon, respectively. This is due to variables such as temperature, water deficit and disturbance regimes. We find that regrowing degraded and secondary forests accumulated 107 Tg C yr^{-1} (90 to 130) between 1984-2018,

counterbalancing 26% (21% to 34%) of carbon emissions from humid tropical forest loss during the same period. Protecting old-growth forests is therefore a priority. Additionally, we estimate that, conserving recovering degraded and secondary forests can have a feasible future carbon sink potential of 53 Tg C yr^{-1} (44 to 62), across the major tropical regions studied.

Main

The Forest and Land use Declaration negotiated at the 26th climate change Conference of the Parties (COP26)[8] confirmed that Tropical Moist Forests (TMF) are a vital nature-based solution to addressing the climate and ecological emergencies[9]. However, across the world's three largest continuous TMF regions – the Amazon, Borneo and Central Africa – disturbances due to different anthropogenic drivers result in ongoing forest cover losses (Supplementary Table 1)[10]. Between 2001 and 2019, emissions from forest loss in the Amazon (370±170 Tg C yr^{-1}), Borneo (150±70 Tg C yr^{-1}), and Central Africa (110±50 Tg C yr^{-1}) collectively made up 29% of global gross forest emissions[11]. The result is a patchwork of forest types at different stages of recovery from disturbance, with limited current understanding of their contribution to forest carbon dynamics.

Here we consider two forest types which we term "Recovering Forests": (i) secondary forests, which grow on deforested, now abandoned, land and (ii) degraded forests, which are forested lands that have suffered partial loss of their tree canopy, structure and function due to selective logging, fire or climate extremes[4]. Forests recovering from (human-induced) disturbances are important for results-based payments frameworks such as Reducing Emissions from Deforestation and Degradation (REDD+). The Global Stocktakes[12], which evaluate the collective progress to reaching the Paris Agreement goals, require credible Monitoring, Reporting and Verification (MRV) of all carbon sources and sinks. This should include accurately quantifying the carbon accumulation rates in all recovering forests, which are expanding across the tropics[4].

Such quantitative information is currently only available for secondary forests, based on field-plot data scaled up to large ecozones[6,13,14] or spatially explicit satellite-based data available only for specific regions[15]. Small-scale studies of carbon recovery in degraded forests have been conducted in some regions with sufficient in-situ data[16,17]. However, field data alone cannot capture the complex forest dynamics across these vast areas. Critically, there has been no large-scale, pan-tropical, assessment of the Aboveground Carbon (AGC) sink in both secondary and degraded forests, resulting in uncertainties in their role in carbon removal. The increasing availability of satellite-derived products offers a viable solution, providing pan-tropical, continuous spatial and temporal coverage, to monitor forest dynamics.

The primary aim of this study was to capture the regrowth variability of all recovering forests in the Amazon, Borneo, and Central Africa, considering each region's unique spatial and temporal patterns of climate, geography, and socio-ecology. We provide the first satellite-based pan-tropical estimates of degraded *and* secondary forest AGC growth rates for these three regions[4]. We (i) quantify the spatial patterns of growth, showing how these are influenced by environmental drivers; (ii) calculate the current and future carbon accumulation potential; (iii) evaluate the timing of deforestation in degraded forests; and (iv) quantify the impact of deforestation on the degraded forests carbon stock potential. We combined a unique satellite dataset, tracking disturbances to the TMF cover (optical, 30m resolution)[4], with a global AGC product (active radar, 100m resolution)[7] in a space-for-time substitution approach to model AGC accumulation as a function of Years Since the Last (forest) Disturbance (YSLD).

Growth of recovering tropical forests

Our analysis of the annual AGC sinks in recovering forests reveals distinct trajectories across the three continents and between forest types (Figure 1). Degraded forests are most severely disturbed in Borneo: after one YSLD, AGC was only 13% of the median AGC of old-growth forests, decreasing from 121 Mg C ha^{-1} (95% confidence interval from Monte Carlo simulations [CI_{MC}]: 119.3 to 122.8) to 16 Mg C ha^{-1} (CI_{MC}: 2.5 to 34.9) (Figure 1a; Supplementary Table 2). In Amazonian and Central African forests, the AGC in newly degraded forests (1 YSLD) was 60.0 (CI_{MC}: 41.6 to 79.1) and 57.3 Mg C ha^{-1} (CI_{MC}: 40.5 to 76.0), respectively. This is approximately 50% the AGC of old-growth forests in the Amazon (121 Mg C ha^{-1} [CI_{MC}: 120.3 to 122.7]) and Central Africa (115 Mg C ha^{-1} [CI_{MC}: 114 to 116]) (Supplementary Table 2; Supplementary Figures 14 to 16).

In the first 20 years of recovery, the average annual growth rate and associated average CI_{MC} of degraded forests in Borneo was 3.60 Mg C ha^{-1} yr^{-1} (CI_{MC}: 2.7 to 4.5). This is 45% and 58% higher than in Central Africa (1.98 Mg C ha^{-1} yr^{-1} [CI_{MC}: 1.8 to 2.2]) and the Amazon (1.49 Mg C ha^{-1} yr^{-1} [CI_{MC}: 1.3 to 1.7]), respectively. In secondary forests, the average growth rate in the first 20 years was similar in Borneo (2.52 Mg C ha^{-1} yr^{-1} [CI_{MC}: 1.3 to 3.7]) and Central Africa (2.51 Mg C ha^{-1} yr^{-1} [CI_{MC}: 1.3 to 3.7]). In the Amazon, the average regrowth rate was 20% lower, but within the CI_{MC} of the other two regions (2.07 Mg C ha^{-1} yr^{-1} [CI_{MC}: 1.2 to 2.9]) (Supplementary Table 4), suggesting there may be higher spatial variability in regrowth across the Amazon.

The observed differences in AGC loss and subsequent regrowth can be linked to the distinct degradation drivers which are dominant in each region (Supplementary Table 1), as well as environmental differences. Notably, the absolute reduction in AGC was highest in Borneo since Indo-Malayan forests are dominated by the ecologically and economically important, high-biomass *Dipterocarpaceae* trees, which grow in high abundance and thus are subject to intense selective logging[18]. The Amazon and Central Africa are dominated by their own ecologically and economically important tree genera, such as the *Entandrophragma* in Central Africa, but at lower abundance, hence forests in these two regions are subject to lower intensity selective logging[19].

Amazonian forests are often degraded by fire, especially in the Brazilian Amazon[17]. Within a fire-degraded forest, there is a complex combination of forest recovery from the initial disturbance, and long-term reductions in AGC due to post-fire mortality[17,20], limiting the overall growth rates.

In degraded forests of Central Africa, the canopy disturbance caused by the dominant, small-scale, manual clearing of individual trees may go undetected by optical remote sensing products estimating land cover change[4]. The active satellite sensors estimating AGC will inherently detect the impact of these small disturbances leading to (i) a potential underestimation in old-growth forest AGC, and (ii) a lower growth rate estimate in recovering degraded forests due to undetected ongoing disturbances (Supplementary Figure 12; Supplementary Note 1; Supplementary Discussion 1).

In contrast, the few secondary forests mapped in Central Africa were regrowing at similar rates to those in the Amazon (Figure 1; Supplementary Table 4) and 1.3 times faster than degraded forests (Supplementary Table 15). The faster annual recovery rate of secondary forests compared to degraded forests may be an artifact of not directly accounting for wood density in our study, which is unique in different recovering forests. Early successional, secondary forests in the humid tropics tend to be fast-growing, low wood-density species, which are gradually replaced by higher wood-density species[21]. Remote sensing datasets do not capture wood density, but rather include wood density intrinsically, thus emphasizing the importance of field validation as we have done here (Supplementary Note 2). Secondary forests, growing in open canopy areas, may also grow faster than degraded forests, where species may still compete for resources such as light and water.

We used the latest, wall-to-wall AGC products that represent the best available data to inform our understanding at large scale. Our regional aggregation approach enabled us to reduce the random errors, which were between 25% to 72% at the pixel level (Supplementary Table 3). However, systematic, or regional biases in the AGC product may still exist (Supplementary Note 1 and 2, Supplementary Discussion 1). For example, our median AGC estimate for old-growth forests was lower than field-study estimates in the three regions (Supplementary Note 1, Supplementary Discussion 1). Exploring these biases is a priority for the AGC field-work and remote sensing communities, with scientific and policy implications.

Across the three regions, we found the AGC of old-growth forests was not statistically different than estimates from a higher resolution (~25m) but spatially limited AGC footprint product (GEDI - Global Ecosystem Dynamics Investigation)[22] (Supplementary Note 1; Supplementary Figure 19), giving confidence that our wall-to-wall estimate is representative of old-growth forest dynamics despite its lower spatial resolution.

A network of pan-tropical ground measurements found Asian secondary forests to have the highest carbon-gains followed by African and then South American forests[23]. Across the three regions, our growth rate estimates, and the AGC after 20 years of recovery in both degraded and secondary forests, are similar to previous studies (Extended Data Figure 1). For example, we calculated that Amazonian secondary forests recovered 37% (CI_{MC}: 36% to 49%) of their AGC relative to old-growth forest AGC after 20 years, similar to 33% found by Poorter et al.[24]. By comparison, we calculated a relative recovery of 62% from a modelling, meta-analysis of field data (Cook-Patton et al.)[14] and using refined regional default values of old-growth forests[25] (Supplementary Note 2; Supplementary Table 18). In the Amazon the Cook-Patton et al. regrowth rates may be at the upper-end of regrowth potential. Despite the high propagated uncertainty in the space-for-time substitution modelling (Supplementary Table 3, Supplementary Discussion 1), the overlaps between different data approaches (satellites and field data) increases our confidence in the likely boundaries of carbon accumulation, and the applicability of satellite products to help refine estimates.

In Borneo, our results for degraded forests are comparable with field-derived estimates of carbon accumulation (2.8 [CI: 2.0 to 3.6] to 4.3 [CI: 3.5 to 5.2] Mg C ha^{-1} yr^{-1}) and recovery times (40 to 60 years) in recovering degraded forests in Malaysian Borneo[16] (Supplementary Note 2). After 40 and 60 years of recovery, we estimated 91% (CI_{MC}: 82% to 99%) and 97% (CI_{MC}: 90% to 102%) of AGC to have recovered, respectively in Bornean degraded forests. Our estimated carbon remaining after degradation (16 Mg C ha^{-1} [CI_{MC}: 2.5 to 34.9] Mg C ha^{-1}) (13%) is low compared to field studies in Borneo (80% AGC remaining after 1 YSLD)[26,27], however the field studies only considered degradation due to logging and no other disturbances such as burning, which we include (Supplementary Note 2; Supplementary Figure 21a to c). We also considered the whole Island, including the southern parts, which have lower AGC density estimates[28] (Supplementary Note 2).

Climate-driven regrowth sensitivity

To understand why the growth of recovering forests varies across the regions, we built AGC growth models stratified by distinct climate conditions (Figure 2 and Extended Data Figure 3) and analysed the response of AGC to different driving variables (Extended Data Figure 2). Across the three regions, YSLD was the most important predictor of AGC accumulation, especially in secondary forests (Extended Data Figure 2), emphasising the importance of long-term conservation for effective climate mitigation.

To investigate the influence of environmental variables, we used the AGC after 20 years of recovery (AGC_{20}) as the primary comparison because growth rates are influenced by both the Y-intercept and asymptotes of the non-linear model. We show that regions with the highest average annual maximum temperatures (Tmax) had significantly slower growth rates compared to regions with the lowest Tmax (10 to 40% slower across all three regions; Figure 2; Supplementary Table 7; Extended Data Figure 2).

In Bornean degraded forests the AGC_{20} was 43% higher in the lowest quartile temperature range (14 to 30.6°C) than in the highest quartile temperature range (31.4 to 32.2°C). This is consistent with previous studies[2,23] and our understanding of tree physiology. Higher temperatures lead to higher Vapour Pressure Deficit, causing leaf stomata closure to avoid water loss[29], and result in lower carbon accumulation.

In Central Africa, the AGC_{20} varied less across the temperature ranges in both degraded and secondary forests. The AGC_{20} was only 15% lower in the warmest region than in the cooler regions (Supplementary Table 7). Growth rates were statistically similar, with overlapping confidence intervals, especially in secondary forests (Supplementary Table 7; Figure 2), potentially owing to the low areal extent of secondary forests mapped in this region (Supplementary Table 15; Figure 1c; Supplementary Discussion 1). African forests may also be more adapted to high temperatures[30] so that other, especially anthropogenic, processes dominate[31].

Across the three regions, recovering degraded and secondary forests in drier areas exhibited 30% lower growth rates than in wetter areas, defined on the basis of the Maximum Cumulative Water Deficit (MCWD) index (Extended Figure 3; Supplementary Table 9). In the Amazon, MCWD significantly influenced AGC recovery (Extended Data Figure 2). The AGC_{20} in Amazonian degraded and secondary forests was 25% and 33% lower in the most water deficient regions (down to –611mm MCWD), respectively than in the least water deficient regions (up to 0mm) (Extended Data Figure 3). The results are consistent with a previous field-based study in the Neotropics, which found secondary forests to have between 20% to 40% lower AGC_{20} in water deficient regions (-300mm to -600mm), than in non-water deficient regions (0mm)[6].

In Borneo, despite being the wettest of three regions in terms of MCWD, the AGC_{20} was 38% lower in the southern, most water deficient parts of the island than in the wetter, northern regions (Extended Data Figure 3c; Supplementary Table 9). The larger drop in growth rates in Borneo is likely because forests are more exposed to extreme drought events caused by El Niño on the southern parts of the island[32]. Bornean forests generally have a narrower water deficit tolerance than other forest regions, thus the rates of carbon accumulation across the whole island may be more vulnerable to extreme drought events[1].

In Central Africa, MCWD had the lowest overall effect in reducing growth rates and associated AGC_{20} (Extended Data Figure 2 and 3) compared to the other two regions. There was only a 13% difference in the growth rates between the lowest and highest MCWD regions in secondary forests. This result, combined with the low response to Tmax, is in line with previous research suggesting (i) that, unlike high temperatures, drought does reduce net carbon uptake in Central African forests[2,30] (Figure 2, Extended Data Figure 2 and 3) but that (ii) overall, forests in Central Africa are more resistant to climate extremes than in the Amazon and Borneo[30], driven in part by more drought-adapted tree species in Central Africa[33].

Based on the consistent differences in AGC accumulation under different climate conditions demonstrated here, we expect a potential reduction in the carbon sink of these forests as a response to future changes in hot and dry climate extremes. Historically, this pattern has been more evident in the Amazon than in Central Africa even though both regions have experienced similar drying patterns and temperature increases over the past decades[34]. Despite recent increased water availability in Asia, forests in this region are more impacted by human-induced disturbances than the other two regions (Figure 1)[34]. We show that generally AGC was less influenced by MCWD and Tmax in secondary forests compared to degraded forests (Extended Data Figure 2). Recovering degraded forests are largely composed of late succession species, which tend to be more sensitive to temperature extremes and drought as the initial disturbance may exacerbate the impact of subsequent extreme events and recurrent, drought-induced, fires[35].

Environment-driven regrowth sensitivity

Our analysis also captured the influence of topography and distance from nearest old-growth forest on secondary and degraded forest regrowth (Extended Data Figure 2). Across the three regions, we found a complicated picture emerging of AGC stock and growth rates with changes in Height Above the Nearest Drainage System (HAND) (Extended Data Figure 2 and 4). Pan-tropically, we found degraded forests had higher growth rates with increased HAND (Extended Data Figure 4; Supplementary Table 11). This relationship was clearest in Borneo, where the AGC_{20} was 34% lower in both degraded and secondary forests growing on floodplains proximal to the river network. This is consistent with some[36], but not all, studies[37] exploring the relationship between topography and AGC. Across all three regions, floodplains include low-lying carbon-rich peatlands that are experiencing extensive deforestation and degradation. In Borneo, lower growth rates in these areas may be due to the difficulties of restoring degraded peatlands due to poor seedbanks, their distinctive hydrology, and species composition[38]. The permanence of the remaining forests, and associated AGC in peatlands, is also at increased risk to further degradation from fire and drought following the initial disturbance as a result of forest fragmentation[39].

Soil and belowground carbon can also be reduced during disturbance. A study of secondary forests in the Neotropics found that soil properties, including soil carbon, recover about 90% of their properties in less than a decade, much faster than AGC[24]. But recovery varies with soil and disturbance type - a study in logged degraded forests in Malaysian Borneo, found soil carbon continued to be lost after AGC recovered[40]. Such studies emphasize the importance of preservation in areas where natural above and below ground regeneration may be slower and the carbon therefore irrecoverable within the 2100 Paris Agreement timesframe[41].

Forest fragmentation across the three regions, represented here by the “distance from the nearest old-growth forest” (see methods) affected the AGC of degraded forests (Extended Data Figure 5; Supplementary Table 13). After one YSLD, degraded forests located closer to old-growth forests had up to 50% higher AGC than more distant degraded forests, presumably related to a lower degree of disturbance in forests proximal to old-growth forests. The AGC_{20} was also up to 50% higher in forests recovering within <120m of an old-growth forest area than in forests growing more than 1km away, despite technical limitations to the approach (Supplementary Discussion 1). Higher growth rates of degraded forests near old-growth forest areas can be attributed to a number of ecological processes, such as increased seed availability, lower fragmentation, and less influence of anthropogenic and climate disturbances such as fires[42] and altered microclimates[1]. We found that the proportion of degraded forests impacted by burning increases with forest fragmentation (Supplementary Figure 21d to f). This was most noticeable in the Amazon region; within 120m of a large old-growth forest cluster, the proportion of degraded forests impacted by burning was 8.4%, this increased to 45% in forests more than 1km away.

Current and future carbon sink potential

Based on our models of carbon accumulation (Figure 1), the total aboveground carbon stored in all recovering forests across the three regions in 2018 equated to 3,559 Tg C (CI_{MC}: 2,994 to 4,290). Most (> 90%) of the 2018 carbon stock of recovering forests was in degraded forests, with two thirds in the three largest countries (Figure 3): Brazil (37%), the Democratic Republic of Congo (DRC; 16%) and Indonesia (14.3%) (Extended Data Figure 6 and 7; Supplementary Figure 18). The area of secondary forests in our study is a conservative estimate in the Brazilian Amazon compared to previous studies (Supplementary Note 1; Supplementary Table 16). Similarly, the area of degraded forests in Borneo and Central Africa is lower than in other datasets (Supplementary Note 1). The characteristics of the data do not impact the analysis of growth rates (per unit area) but the estimated total carbon contribution from all recovering forests is likely underestimated.

The spatial pattern of carbon stock followed the areas which have experienced severe human-disturbances, such as the "Arc of deforestation" in the Brazilian Amazon and along logging roads in Central Africa and Borneo. These could be indicative areas of focus for the UN 2021-2030 decade of ecosystem restoration (Figure 3). Our results show that secondary and degraded forests across the Amazon collectively store 2,124 Tg C (CI_{MC}: 1808 to 2541) (annual sink of 62 Tg C yr^{-1} [CI_{MC}: 53 to 75]). Owing largely to the Amazon's vast spatial extent (Figure 3), the carbon stored is approximately 65% higher there than in Borneo (729 Tg C [CI_{MC}: 589 to 913], where we estimate an annual sink of 24 Tg C yr^{-1} [CI_{MC}: 19 to 30]).

Central Africa has the lowest total carbon storage in recovering forests (707 Tg C [CI_{MC}: 597 to 836]), (Figure 3c), despite being the second largest of the three regions. The low carbon sink (21 Tg C yr^{-1} [CI_{MC}: 18 to 25]) is likely linked to the fact that human impact on forest cover often occurs below the spatial scale detectable by the remote sensing products (Supplementary Figure 12). Monitoring and protecting the remaining old-growth forest in Central Africa may therefore be more important for project-scale carbon policies and frameworks such as REDD+[43]. Central Africa has the fastest growing population of the three regions, anthropogenic pressures such as continued population growth are, therefore, likely to have the largest impact on forest carbon loss by the end of the 21st century, which will be exacerbated by climate change[31].

Our results emphasise that the type of REDD+ activities should not be uniform across the tropics. Such results can be used to inform international funders and empower local, community-led efforts to sustainably manage and protect recovering forests in a targeted manner, addressing the local drivers of unsustainable forests loss, whilst allowing people and biodiversity to thrive[44].

So far we have only accounted for the carbon gains in recovering forests, however, rates of deforestation and degradation in the tropics remain high (Supplementary Figure 13), with a recent increasing trend in some regions[4]. We estimated that across the tropics, the AGC accumulated in recovering forests (3,560 Tg C [CI_{MC}: 2994 to 4290]) counterbalanced 26% (CI_{MC}: 21% to 34%) of the gross AGC emissions from deforestation (10,521 Tg C [CI_{MC}: 10,441 to 10,655]) and degradation (2,916 Tg C [CI_{MC}: 2,157 to 3,602]) between 1984 to 2018 (Extended Data Table 1). The emissions estimated from degradation are about 28% of deforestation-based emissions. This is similar to a previous study focusing on selective logging[45]. Furthermore, we found about 35% of degraded forests were deforested by 2018 (Extended Data Table 2). If these degraded forests had been preserved, the potential contribution from all recovering forests (5,892 Tg C [CI_{MC}: 5,114 to 6,842]) to counterbalance gross forest loss emissions (12,349 Tg C [CI_{MC}: 11,714 to 13,787]) could have reached 48% (37% to 58%) (Extended Data Table 2).

Based on the existing 2018 carbon stocks of recovering forests and our estimated rates of carbon accumulation (Figure 1), we modelled the potential carbon gain by 2030 for the three regions assuming all recovering forests were protected and regrow (Figure 4). We calculate a potential future carbon sink of 1,149 Tg C (CI_{MC}: 1010 to 1,288), a 32% increase from the 2018 carbon stock (Figure 4). Thus, protecting the remaining recovering forests not only maintains carbon stock, but also maximizes the carbon sink potential. However, this maximum potential value is likely unfeasible. Many secondary forests are part of long-standing shifting cultivation practices, and degraded forests in logging concession areas are typically cut in 15 to 40 year cycles or converted to other land uses[46]. Of the degraded forests that were later deforested (35%), we found that almost half (44% to 47%) were deforested within the first 5 years after their last disturbance event (Supplementary Figure 17), suggesting that recently degraded forests are most at risk from further deforestation, making their carbon stock potentially more “vulnerable”. Recently disturbed forests covered a larger area than older recovering forests (Supplementary Figure 13) and contained 29% (Borneo) to 60% (Central Africa) of the modelled recovering forest carbon stock potential in 2030 (Figure 4; Supplementary Figure 18). Deciding which recovering forests to protect is therefore not straight forward.

A more feasible scenario for calculating potential of conservation may be to ensure that at least recently (<6 YSLD) degraded forests and older (>20 YSLD+) secondary forests are allowed to recover to 2030. The combined carbon gain in such a scenario would be 639 Tg C (CI_{MC}: 533 to 744) across the three regions, equivalent to ~56% of the maximum technical future carbon sink potential (1,149 Tg C). Limiting subsequent deforestation of recently degraded forests, increasing the interval between anthropogenic disturbances, such as logging, and reducing the intensity of the disturbance would ensure these forests can continue to be used sustainably by the people that depend on them[27].

Our calculations demonstrate that the large-scale, maximum technical carbon sink potential may not be realised at the local scale as not all forests recover from disturbance. Studies have shown that degraded forests disturbed by fire, continue to be a net source of carbon for many years following the initial disturbance due to legacy fluxes, post-fire disease and mortality[20]. Future remote sensing studies could identify where large-scale carbon losses continue following the initial disturbance. Such an approach, combined with identification of forests according to the YSLD, as we have done here, may help to prioritise areas for conservation and restoration.

Recovering forests can continue to provide ecosystem services. Degraded forests in Malaysian Borneo were found to provide access to clean water, clean air and regulate temperature[47]. Older secondary forests can increase biodiversity in both species’ richness and diversity[48]. In some places, older secondary forests even gain protected status after a certain number of years[49]. However, the efforts to protect secondary and degraded forests cannot be at the expense of the conservation of old-growth forests, which remains the most cost-effective climate mitigation strategy in the land-use sector[50]. Old-growth forests continue to be subject to unsustainable rates of deforestation and degradation, and emissions from old-growth forest deforestation (10,521 Tg C) and degradation (2,916 Tg C) still greatly outweigh the removals from recovery (3,560 Tg C) (Extended Data Table 1).

The priority for meeting the declaration on forest conservation (COP26)[8] therefore remains protecting old-growth forests. Nevertheless, our study provides the first pan-tropical quantitative evidence that recovering degraded forests are a sizeable carbon sink, despite the slow, decade to centennial-timescale of the recovery process. It is therefore important to invest in sustainably conserving recovering forests, to safeguard their current and future carbon sink potential.

References [main]

1. Qie, L. *et al.* Erratum: Author Correction: Long-term carbon sink in Borneo’s forests halted by drought and vulnerable to edges (Nature communications (2017) 8 1 (1966)). *Nat. Commun.* **9**, 342 (2018).
2. Hubau, W. *et al.* Asynchronous carbon sink saturation in African and Amazonian tropical forests. *Nature* **579**, 80–87 (2020).
3. Gatti, L. V. *et al.* Amazonia as a carbon source linked to deforestation and climate change. *Nature* **595**, (2021).
4. Vancutsem, C. *et al.* Long-term (1990–2019) monitoring of forest cover changes in the humid tropics. *Sci. Adv.* **7**, eabe1603 (2021).
5. Chazdon, R. L. *et al.* Carbon sequestration potential of second-growth forest regeneration in the Latin American tropics. *Sci. Adv.* **2**, e1501639 (2016).
6. Poorter, L. *et al.* Biomass resilience of Neotropical secondary forests. *Nature* **530**, 211–214 (2016).
7. Santoro, M. & Cartus, O. ESA Biomass Climate Change Initiative (Biomass_cci): Global datasets of forest above-ground biomass for the years 2010, 2017 and 2018, v2. *Centre for Environmental Data Analysis* http://dx.doi.org/10.5285/84403d09cef3485883158f4df2989b0c (2021) doi:10.5285/84403d09cef3485883158f4df2989b0c.
8. COP26, G. U. Glasgow Leaders’ Declaration on Forests and land use. https://ukcop26.org/glasgow-leaders-declaration-on-forests-and-land-use/ (2021).
9. Seddon, N. Harnessing the potential of nature-based solutions for mitigating and adapting to climate change. *Science (80-.).* **376**, 1410–1416 (2022).
10. Curtis, P. G., Slay, C. M., Harris, N. L., Tyukavina, A. & Hansen, M. C. Classifying drivers of global forest loss. *Science (80-.).* **361**, 1108–1111 (2018).
11. Harris, N. L. *et al.* Global maps of twenty-first century forest carbon fluxes. *Nat. Clim. Chang.* **11**, 234–240 (2021).
12. UNFCCC. Global Stocktake. https://unfccc.int/topics/global-stocktake (2015).
13. Requena Suarez, D. *et al.* Estimating aboveground net biomass change for tropical and subtropical forests: Refinement of IPCC default rates using forest plot data. *Glob. Chang. Biol.* **25**, 3609–3624 (2019).
14. Cook-Patton, S. C. *et al.* Mapping carbon accumulation potential from global natural forest regrowth. *Nature* **585**, 545–550 (2020).
15. Heinrich, V. H. A. *et al.* Large carbon sink potential of secondary forests in the Brazilian Amazon to mitigate climate change. *Nat. Commun.* **12**, 1785 (2021).
16. Philipson, C. D. *et al.* Active restoration accelerates the carbon recovery of human-modified tropical forests. *Science (80-.).* **369**, 838–841 (2020).
17. Rappaport, D. I. *et al.* Quantifying long-term changes in carbon stocks and forest structure from Amazon forest degradation. *Environ. Res. Lett.* **13**, (2018).
18. Hayward, R. M. *et al.* Three decades of post-logging tree community recovery in naturally regenerating and actively restored dipterocarp forest in Borneo. *For. Ecol. Manage.* **488**, 119036 (2021).

19. Putz, F. E. *et al.* Intact Forest in Selective Logging Landscapes in the Tropics. *Front. For. Glob. Chang.* **2**, (2019).

20. Silva, C. V. J. *et al.* Estimating the multi-decadal carbon deficit of burned Amazonian forests. *Environ. Res. Lett.* **15**, (2020).

21. Poorter, L. *et al.* Wet and dry tropical forests show opposite successional pathways in wood density but converge over time. *Nat. Ecol. Evol.* **3**, 928–934 (2019).

22. Dubayah, R. *et al.* The Global Ecosystem Dynamics Investigation: High-resolution laser ranging of the Earth's forests and topography. *Sci. Remote Sens.* **1**, (2020).

23. Sullivan, M. J. P. *et al.* Long-term thermal sensitivity of earth's tropical forests. *Science (80-.).* **368**, 869–874 (2020).

24. Poorter, L. *et al.* Multidimensional tropical forest recovery. *Science (80-.).* **374**, 1–8 (2021).

25. Rozendaal, D. *et al.* Aboveground forest biomass varies across continents, ecological zones and successional stages: refined IPCC default values for tropical and subtropical forests. *Environ. Res. Lett.* **17**, 014047 (2022).

26. Griscom, B., Ellis, P. & Putz, F. E. Carbon emissions performance of commercial logging in East Kalimantan, Indonesia. *Glob. Chang. Biol.* **20**, 923–937 (2014).

27. Putz, F. E. *et al.* Sustaining conservation values in selectively logged tropical forests: The attained and the attainable. *Conserv. Lett.* **5**, 296–303 (2012).

28. Avitabile, V. *et al.* An integrated pan-tropical biomass map using multiple reference datasets. *Glob. Chang. Biol.* **22**, 1406–1420 (2016).

29. Lloyd, J. & Farquhar, G. D. Effects of rising temperatures and [CO2] on the physiology of tropical forest trees. *Philos. Trans. R. Soc. B Biol. Sci.* **363**, 1811–1817 (2008).

30. Bennett, A. C. *et al.* Resistance of African tropical forests to an extreme climate anomaly. *Proc. Natl. Acad. Sci.* **118**, e2003169118 (2021).

31. Ross, C. W. *et al.* Woody-biomass projections and drivers of change in sub-Saharan Africa. *Nat. Clim. Chang.* **11**, 449–455 (2021).

32. Esquivel-Muelbert, A. *et al.* A spatial and temporal risk assessment of the impacts of El Niño on the tropical forest carbon cycle: Theoretical framework, scenarios, and implications. *Atmosphere (Basel).* **10**, (2019).

33. Zhou, L. *et al.* Widespread decline of Congo rainforest greenness in the past decade. *Nature* **508**, 86–90 (2014).

34. Saatchi, S. *et al.* Detecting vulnerability of humid tropical forests to multiple stressors. *One Earth* **4**, 988–1003 (2021).

35. Brando, P. M. *et al.* Abrupt increases in Amazonian tree mortality due to drought-fire interactions. *Proc. Natl. Acad. Sci. U. S. A.* **111**, 6347–6352 (2014).

36. Ferraz, A. *et al.* Carbon storage potential in degraded forests of Kalimantan, Indonesia. *Environ. Res. Lett.* **13**, (2018).

37. Jucker, T. *et al.* Topography shapes the structure, composition and function of tropical forest landscapes. *Ecol. Lett.* **21**, 989–1000 (2018).

38. Blackham, G. V., Webb, E. L. & Corlett, R. T. Natural regeneration in a degraded tropical

peatland, Central Kalimantan, Indonesia: Implications for forest restoration. *For. Ecol. Manage.* **324**, 8–15 (2014).

39. Nikonovas, T., Spessa, A., Doerr, S. H., Clay, G. D. & Mezbahuddin, S. Near-complete loss of fire-resistant primary tropical forest cover in Sumatra and Kalimantan. *Commun. Earth Environ.* **1**, 1–8 (2020).

40. Riutta, T. *et al.* Major and persistent shifts in below-ground carbon dynamics and soil respiration following logging in tropical forests. *Glob. Chang. Biol.* **27**, 2225–2240 (2021).

41. Noon, M. L. *et al.* Mapping the irrecoverable carbon in Earth's ecosystems. *Nat. Sustain.* **5**, 37–46 (2022).

42. Rosan, T. M. *et al.* Fragmentation-Driven Divergent Trends in Burned Area in Amazonia and Cerrado. *Front. For. Glob. Chang.* **5**, 1–10 (2022).

43. Poulsen, J. R. *et al.* Old growth Afrotropical forests critical for maintaining forest carbon. *Glob. Ecol. Biogeogr.* **29**, 1785–1798 (2020).

44. Haenssgen, M. J. *et al.* Implementation of the COP26 declaration to halt forest loss must safeguard and include Indigenous people. *Nat. Ecol. Evol.* **6**, 235–236 (2022).

45. Maxwell, S. L. *et al.* Degradation and forgone removals increase the carbon impact of intact forest loss by 626%. *Sci. Adv.* **5**, (2019).

46. Reynolds, G., Payne, J., Sinun, W., Mosigil, G. & Walsh, R. P. D. Changes in forest land use and management in Sabah, Malaysian Borneo, 1990-2010, with a focus on the Danum Valley region. *Philos. Trans. R. Soc. B Biol. Sci.* **366**, 3168–3176 (2011).

47. Boul Lefeuvre, N. *et al.* The value of logged tropical forests: A study of ecosystem services in Sabah, Borneo. *Environ. Sci. Policy* **128**, 56–67 (2022).

48. Lennox, G. D. *et al.* Second rate or a second chance? Assessing biomass and biodiversity recovery in regenerating Amazonian forests. *Glob. Chang. Biol.* **24**, 5680–5694 (2018).

49. Vieira, I. C. G., Gardner, T., Ferreira, J., Lees, A. C. & Barlow, J. Challenges of governing second-growth forests: A case study from the Brazilian Amazonian state of Pará. *Forests* **5**, 1737–1752 (2014).

50. Roe, S. *et al.* Land-based measures to mitigate climate change: Potential and feasibility by country. *Glob. Chang. Biol.* **27**, 6025–6058 (2021).

Methods

Recovering forest carbon accumulation

The primary dataset used in this analysis was the pantropical dataset that monitors the extent and changes in Tropical Moist Forests (TMF) over the last three decades[4]. TMF includes all closed forests (>90% crown cover) in humid forests only. This TMF dataset is based on observations of the Landsat collection from 1982 to 2019, where available, with a spatial scale of 30m and an annual temporal frequency over 38 years. Importantly, this dataset characterises the duration of the observations of tree cover disturbances, enabling disturbances to be classified as either forest degradation events (disturbances that are visible for less than 2.5 years) or deforestation events (disturbances that last for more than 2.5 years). A disturbance observation was defined as the absence of tree cover in a pixel that had previously been characterised as TMF cover. From this approach it was possible to map degraded forests and secondary forests, amongst other forest cover types. Degraded forests were defined here as tree covered pixels where disturbances were visible for a short time period (between 3 months and 2.5 years maximum) whereas secondary forests were defined as pixels with natural regrowing vegetation after an absence of tree cover for more than 2.5 years.

The TMF dataset can be used to estimate the time (in years) since the last disturbance event for any recovering forests, which was considered as a good proxy of the age of secondary forests in this study (Supplementary Figure 10). We used the extent of the different forest types and the metric "Years Since Last Disturbance" (YSLD) as the first input data in this research. The second key input data used in this study was the ESA-CCI Aboveground Biomass (AGB) dataset, available for the year 2018[7]. We converted the AGB into Aboveground Carbon (AGC) by applying a conversion factor of 0.456[51]. The TMF and AGC dataset were combined to determine the AGC with increasing YSLD in a space-for-time substitution approach, a method that was applied by Heinrich et al (2021)[15]. As the AGC dataset extends only to 2018, the TMF dataset was pre-processed to extract a map of YSLD in 2018 for degraded and secondary forests, respectively within the three main continuous tropical humid forests regions, the Amazon, Island of Borneo, and Central Africa. We opted not to expand the analysis to include broader regions such as the Neotropics, Western Africa and Southeast Asia more generally as this would encompass many smaller, and often insular, landscapes, adding further complexity to the already heterogenous environmental and anthropogenic drivers.

The possible range of YSLD was from 1 to 36 years, however due to limited availability in the early collection of satellite imagery (i.e. in the 1980s and 1990s) this range was lower, in the three regions, the oldest degraded/secondary forests were 34 years old (i.e. growing since 1984)[4]. Using ArcGIS Pro (Python 3.6.10; arcpy)[52] we grouped connected forest pixels into forest type clusters, based on the YSLD and extracted the forest clusters with more than nine pixels (i.e., clusters with an area greater than 0.81 ha). This is an area approximately equal to one pixel of the ESA-CCI product (100m spatial scale). Following the removal, over 8.7 million clusters were available for analysis (Supplementary Table 15) for which the modal AGC was determined for each forest cluster.

In addition we used a pan-tropical dataset of commercial and small holder oil palm cover available for the year 2019[53] to remove oil palm plantations from the TMF secondary or degraded forests. This was particularly important for Borneo, where there are large areas of small holder oil palm plantations that are partly misclassified as forest regrowth in the TMF dataset. We removed all areas that are classified as any type of oil palm in this ancillary dataset.

Following this correction we carried out our post-processing analysis in the statistical software programme R (v4.0.2)[54] (Supplementary Table 17). We calculated the median AGC value per forest YSLD. When applying this analysis for the secondary forest type we applied a bias correction to the AGC values for each YSLD by subtracting the smallest AGC value from all values such that the data began at or near 0 Mg C ha^{-1} for a 1 year-old secondary forest[15]. We did not apply this kind of bias correction to the degraded forest as we assumed that even after 1 YSLD the degraded forests would retain some level of AGC post-disturbance.

Following a similar approach to Heinrich et al[15] that used a space-for-time substitution approach to model AGC accumulation with increasing forest age across the Brazilian Amazon[15], we modelled the AGC accumulation with increasing YSLD using the Chapman-Richard model for growth[55] within each of the three rainforest regions:

$$Y_t = A(1-e^{-kt})^c \pm \varepsilon;\ A,\ k,\ \text{and}\ c > 0 \qquad (1)$$

Where Y_t refers to the AGC at YSLD (t); A is the AGC asymptote or the AGC of the old-growth forest; k is a growth rate coefficient of Y as a function of age; c is a coefficient that determines the shape of the growth curve; and ε is an error term. We assumed that after a given number of years, the AGC could return to levels equivalent to old-growth forests and reach a precalculated asymptote. We therefore extracted the AGC values corresponding to undisturbed forest pixels in the TMF map of year 2018 that are here considered as a proxy for old-growth forests. The median AGC value of undisturbed forest pixels were then used as the A term in equation (1). We then compared our estimates of growth rates with estimates from previous studies[14,16] and did a detailed comparison with estimates of secondary forest growth in the Brazilian Amazon (Supplementary Note 1)[15,56–58]. The Brazilian Amazon was chosen to carry out the in-depth analysis as this is a region with extensive previous research, with in-country remote sensing datasets for comparison. Where studies indicated the conversion factor used to convert AGB to AGC we adjusted these to reflect the conversion factor used in this study (0.456)[51].

Modelling carbon accumulation by drivers

Over the period 1985 to 2018, we calculated the average of two climate variables that are known to have an impact on forest dynamics to model the AGC under varying conditions of the variables: the average maximum annual temperature (Tmax)[59] and the Maximum Cumulative Water Deficit (MCWD), which is often used as an indicator of drought[60–62]. Additionally, we investigated the impact that a normalised terrain model (Height Above Nearest Drainage; HAND) had on the growth rates[63]. A further variable we investigated was the distance from nearest region of old-growth forest as a proxy for forest fragmentation, which we developed in this study using the TMF dataset[4]. The two climate variables were chosen to enable the most direct comparison with previous studies that have also used these variables [15,23,30], enabling us to benchmark and validate our approach. The two environmental variables, HAND and distance from undisturbed forest, were chosen as the impact of these variables has only been explored in a few region-specific studies but never across the pan-tropics, thus providing new scientific insights.

To determine the distance between degraded or secondary forest areas and old-growth (i.e., undisturbed) forests we first identified and extracted clusters of connected pixels of old-growth forest with an area of more than 6.25ha. We did this as to exclude small patches of old-growth forest. The threshold of 6.25ha, equal to ca. 70 pixels of the TMF dataset, was chosen as this is the minimum area detected by the PRODES deforestation mask developed by the National Institute for Space Research (INPE) in Brazil, which produces annual maps of deforestation in the Brazilian Legal Amazon[64]. We then expanded the perimeter of old-growth forest clusters by 4 (~120m), 17 (~500m), 33 (~1000m) and 67 (~2000m) pixels and aggregated the layers together to produce a map of distance from large old-growth forests.

We determined the modal value of the respective variables overlying either the degraded or secondary forest pixel within a region of the same YSLD. In R we calculated the corresponding percentile of each variable value weighted by the number of connected pixels within a forest region. We split the dataset into the forest regions that experienced the lowest 25%, middle 50% and upper 75% of the respective variables. The only variable for which we manually created the groups was the "distance from old-growth forest" as the forest regions were generally heavily skewed to being close to the old-growth forests. We therefore manually created three groups: (i) "< 120m"; (ii) "120m to 1000m"; and (iii) "1000m +" to represent distance (in metres) from nearest large patch of old-growth forest. In each of these groups we again calculated the median AGC value per forest YSLD, weighted by the number of connected pixels within a forest region. Finally, we applied equation 1 within the nls function again to model the growth in the different forest types, this time split up by the variable quartiles.

Modelling the importance of each driver

We used a multi-linear model approach to relate AGC to the independent variables as well as the YSLD within the three regions. The relative importance of each independent variable in influencing AGC was assessed using a bootstrapping approach. Prior to this we assessed whether the variables had (i) a linear-relationship with AGC and (ii) if any of the variables had a colinear relationship with another driver using various correlation coefficients such as Pearson's R and Spearman's rho as well as the linear model's Variance Inflation Factor (VIF) analysis. Where the correlation coefficients were below ±0.5 and VIF values were < 2, we assumed the relationship between the independent variables was not very strongly correlated and therefore could be used in the modelling analysis (Supplementary Figure 3 and 4). Based on the assessment of linearity, we also concluded that there were no relationships with AGC that were clearly non-linear (Supplementary Figure 5, 6 and 7), and so we assumed a linear relationship of all the variables with AGC and scaled the variables to between 0 – 1 to enable comparison between the regions. Although we assumed a non-linear relationship of AGC with time (YSLD) in Equation 1, many of our comparisons to previous studies used the average growth rate in the first 20 years since the last disturbance event, a linear interpretation of growth that we also applied in this analysis.

In order to minimize spatial autocorrelation when building the linear model[65] we built an exponential semi-variogram model, to test at what distance (in degrees) the linear model residuals were no longer spatially autocorrelated. We estimated that a distance of 0.5 degrees (~55 km) for the Amazon and Central Africa and 0.3 degrees (~33 km) for Borneo minimized spatial autocorrelation and that this information could be used in a stratified spatial sampling approach[66]. We rounded the latitude and longitude coordinates of each forest cluster to the nearest 0.5 (0.3) degrees and then sampled the data such that only 1 forest cluster of each 0.5 (0.3) grid square was selected for further analysis.

We then applied the linear model to determine the standardised coefficients of each of the environmental variables as well as YSLD in each forest type within each region. We ran the linear model analysis 100,000 times, randomly sampling a forest cluster per grid square at each iteration. Next, we calculated the average coefficient, standard error, and p-value at the 95% confidence interval for each variable across all the iterations.

Mapping regional carbon stock potential

To map the carbon stock potential, we applied the region-specific growth models to all secondary and degraded forest pixels respectively. We calculated the accumulated carbon stock of the standing area of recovering forest in 2018 and produced a map, aggregated to 0.1-degree grid square of the 2018 carbon stock. Here we also show the regions identified as peatland[67,68], to highlight where there may be additional soil carbon benefits. We also applied a similar approach to Chazdon et al.[5] and modelled the potential carbon stock at the end of 2030 if all the 2018 standing forest remained standing and were protected until the year 2030. We disaggregated the information by forest type and by country within the regions to demonstrate the carbon stock that can be lost if the forests were not left to stand, but also the carbon that could be gained if the forests are protected.

Estimating forest carbon losses

We estimated the gross carbon losses from deforestation and degradation in the following manner:

(i) For the carbon losses from deforestation, we used the TMF dataset to identify the year a forest pixel was deforested. The total area that was deforested between 1984 and 2018 across the three regions was multiplied by the median AGC value of old-growth forest, assuming that all AGC would be lost. This provided the total amount of AGC lost due to deforestation over the study period. Old-growth forests that were first degraded and then subsequently deforested are included in this estimate.

(ii) For the carbon losses from degradation we used the difference between AGC in old-growth forests and the modelled AGC in areas after the first year since the last disturbance event (i.e., 1 YSLD). We took these differences as the emission factor for degraded forests across the respective regions and multiplied it by the area of degraded forests in 2018 to estimate the total AGC loss due to degradation.

Model variability and uncertainty

We used more than 8.7 million secondary and degraded forest connected pixel clusters across the three study regions, using their median to estimate the changes in AGC with YSLD. The use of remote sensing data has the potential to capture the spatial variability in regrowth across these dynamic regions, which is in part masked when taking the median value across the whole region.

We aimed to disaggregate this variability by environmental variables, but also wanted to demonstrate the range of recovery aggregated across the three regions by running 50 Monte Carlo simulations. Each simulation randomly sampled the data such that a total of ~10% of the dataset was sampled at the end of the simulations. This was equivalent to sub-sampling 100 and 25 clusters for each YSLD group for degraded and secondary forests, respectively. In each simulation we applied the methodology described above, calculating the median AGC per YSLD group, applying Equation 1 and determining the 95% confidence interval. We also estimated a new old-growth forest AGC value to represent the asymptote based on randomly sampled pixels of old-growth forest AGC. We then estimated the 95% confidence interval from the Monte Carlo simulations to represent the model variability (Supplementary Figure 14 to 16; Supplementary Table 2).

We estimated the uncertainty caused by the ESA-CCI dataset of AGB, a parameter which is provided on a pixel-scale in the dataset as the standard error. We followed a similar methodology when extracting the mean AGB values for each cluster, by determining the modal standard error for each cluster of a specific YSLD. We calculated the median standard error value for each YSLD grouping in each region. We then propagated the error of the dataset ($Data_{SE}$) with the error of the fitted regional models. The non-linear growth model provided an estimate of the uncertainty expressed as both the 95% confidence interval and the residual standard error. We propagated the residual standard error of the model ($Model_{SE}$) with $Data_{SE}$ using the root square of sum method to obtain an overall standard error of the regional growth models (Supplementary Table 3).

Supplementary information

Supplementary Information is available for this paper.

Data Availability

All the original datasets used in this research are publicly available from their sources: JRC-TMF dataset[4] (https://forobs.jrc.ec.europa.eu/TMF/download/); ESA-CCI AGB/AGC map[7] (https://catalogue.ceda.ac.uk/uuid/84403d09cef3485883158f4df2989b0c); Descal et al. (2021) oil palm map[53] (https://developers.google.com/earth-engine/datasets/catalog/BIOPAMA_GlobalOilPalm_v1#description); TerraClimate Maximum Temperature[59] (https://developers.google.com/earth-engine/datasets/catalog/IDAHO_EPSCOR_TERRACLIMATE); MCWD data can be produced by combining monthly rainfall dataset from Funk et al.[61] (https://edcintl.cr.usgs.gov/downloads/sciweb1/shared/fews/web/global/monthly/chirps/final/downloads/monthly/) with code from Campanharo and Silva Junior (2019)[60]; HAND data[69] (https://code.earthengine.google.com/ed75ecef7fcf94897b74ac56bfbb3f43); Xu et al. Peatland dataset[67] (https://archive.researchdata.leeds.ac.uk/251/); MapBiomas dataset[70] (https://amazonia.mapbiomas.org/) and the code to extract secondary forest area and age[58]; Logging concession areas[71] (https://data.globalforestwatch.org/datasets/managed-forest-concessions/explore). Both the Tmax and HAND indices were pre-processed in GEE. Country boundaries shown in map-based figures (http://thematicmapping.org/downloads/world_borders.php)[72]

All final data produced in this study are available in a public repository: https://zenodo.org/record/7330549#.Y3vCo0nP1PY [73]

Code Availability

All code used to produce the main figures of the are available in a public repository: https://zenodo.org/record/7330549#.Y3vCo0nP1PY [73]

References [Methods]

51. Martin, A. R., Doraisami, M. & Thomas, S. C. Global patterns in wood carbon concentration across the world's trees and forests. *Nat. Geosci.* **11**, 915–920 (2018).

52. ESRI. ArGIS Pro Desktop (2.6.0). (2020).

53. Descals, A. *et al.* High-resolution global map of smallholder and industrial closed-canopy oil palm plantations. *Earth Syst. Sci. Data* **13**, 1211–1231 (2021).

54. R Development Core Team. R: A Language and Environment for Statistical Computing. (2008).

55. Richards, F. J. A flexible growth function for empirical use. *J. Exp. Bot.* **10**, 290–301 (1959).

56. Smith, C. C. *et al.* Secondary forests offset less than 10% of deforestation-mediated carbon emissions in the Brazilian Amazon. *Glob. Chang. Biol.* 1–15 (2020) doi:10.1111/gcb.15352.

57. Nunes, S., Jr. Oliveira, L., Siqueira, J., Morton, D. C. & Souza, C. M. Unmasking secondary vegetation dynamics in the Brazilian Amazon. *Environ. Res. Lett.* **15**, (2020).

58. Silva Junior, C. H. L. *et al.* Benchmark maps of 33 years of secondary forest age for Brazil. *Sci. Data* **7**, 269 (2020).

59. Abatzoglou, J. T., Dobrowski, S. Z., Parks, S. A. & Hegewisch, K. C. TerraClimate, a high-resolution global dataset of monthly climate and climatic water balance from 1958-2015. *Sci. Data* **5**, 1–12 (2018).

60. Campanharo, W. & Silva Junior, C. H. L. Maximun Cumulative Water Deficit - MCWD: a R language script. (2019) doi:10.5281/zenodo.2652629.

61. Funk, C. *et al.* The climate hazards infrared precipitation with stations - A new environmental

record for monitoring extremes. *Sci. Data* **2**, 1–21 (2015).

62. Phillips, O. L. *et al.* Drought Sensitivity of the Amazon Rainforest. *Science (80-.).* **323**, 1344–1347 (2009).

63. Nobre, A. D. *et al.* Height Above the Nearest Drainage - a hydrologically relevant new terrain model. *J. Hydrol.* **404**, 13–29 (2011).

64. Almeida, C. A. *et al.* High spatial resolution land use and land cover mapping of the Brazilian legal Amazon in 2008 using Landsat-5/TM and MODIS data. *Acta Amaz.* **46**, 291–302 (2016).

65. Ploton, P. *et al.* Spatial validation reveals poor predictive performance of large-scale ecological mapping models. *Nat. Commun.* **11**, 1–11 (2020).

66. Haining, R. . Spatial Sampling. in *International Encyclopedia of the Social and Behavioral Sciences* (eds. Smelser, N. & Baltes, P.) 14822–14827 (Pergamon, 2001).

67. Xu, J., Morris, P. J., Liu, J. & Holden, J. PEATMAP: Refining estimates of global peatland distribution based on a meta-analysis. *Catena* **160**, 134–140 (2018).

68. Xu, J., Morris, P. J., Liu, J. & Holden, J. Dataset: PEATMAP: Refining estimates of global peatland distribution based on a meta-analysis. https://archive.researchdata.leeds.ac.uk/251/ (2017) doi:10.5518/252.

69. Donchyts, G., Winsemius, H., Schellekens, J., Erickson, T. & Gao, H. Global 30m Height Above the Nearest Drainage. *Geophys. Res. Abstr.* **18**, (2016).

70. Souza, C. M. *et al.* Reconstructing three decades of land use and land cover changes in brazilian biomes with landsat archive and earth engine. *Remote Sens.* **12**, (2020).

71. Global Forest Watch. Managed Forest concessions. www.globalforestwatch.org (2020).

72. ThematicMapping. http://thematicmapping.org/downloads/world_borders.php (2009).

73. Heinrich, V. H. A. *et al.* Data and code from paper: The carbon sink of recovering degraded and secondary tropical forests. https://zenodo.org/record/7330549#.Y3vCo0nP1PY (2022) doi:10.5281/zenodo.7330548.

Acknowledgements

We thank A. Esquivel-Muelbert and E. Mitchard for their valuable input during the preparation of this manuscript. We thank M.Brasika, A.Jumail, H.R.Yen, C.Cheng, L.Mercado, J.Echeverría and M.Heinrich for translating the Summary Paragraph. V.H.A.H. was supported by a NERC GW4+ Doctoral_Training Partnership studentship from the Natural Environment Research Council (NE/L002434/1). R.D. was supported by São Paulo Research Foundation (FAPESP) grant 2019/21662-8. T.J. was supported by a UK NERC Independent Research Fellowship (NE/S01537X/1). V.H.AH, T.R., D.F. and S.S. were supported by the RECCAP2 project which is part of the ESA Climate Change Initiative (contract no. 4000123002/18/I-NB) and the H2020 European Institute of Innovation and Technology (4C; grant no. 821003). H.L.G.C. was supported by São Paulo Research Foundation (FAPESP) grant #2018/14423-4 and 2020/02656-4. C.V. was supported by the Directorate General for Climate Action of the European Commission through the ForMonPol (Forest Monitoring for Policies) Administrative Arrangement. C.H.L.S.J. was supported by The University of Manchester through the "Forest Haproject. We thank the School of Geographical Sciences, University of Bristol for their additional support. This research was funded in part by Natural Environment Research

Council (NE/L002434/1). For the purpose of open access, the author has applied a ‘Creative Commons Attribution (CC BY) public copyright license to any Author Accepted Manuscript (AAM) version arising from this submission.

Author Contributions

V.H.A.H., J.H, S.S., T.C.H., and L.E.O.C.A designed the concept and methodological process of the study. V.H.A.H carried out the main data analysis with support from R.D., D.F, T.M.R., C.H.L.S.J., H.L.G.C. and T.J.. C.V. provided the code for analysis and the data of the Tropical Moist Forest dataset prior to the publication of the study with guidance from F.A.. C.A.S processed the raw GEDI data for further analysis. V.H.A.H wrote the initial draft of the manuscript. All authors (V.H.A.H., C.V., R.D., T.M.R., D.F., C.H.L.S.J., H.L.G.C., F.A., T.J., C.A.S., J.H., S.S., T.C.H., and L.E.O.C.A) discussed results, provided comments during the preparation of the manuscript, and gave their approval for

Competing interest declaration

The authors declare no competing interests, financial or otherwise.

Correspondence and request for material should be addressed to V.H.A.H.

Reprints and permissions information is available at www.nature.com/reprints

Display Material Legends

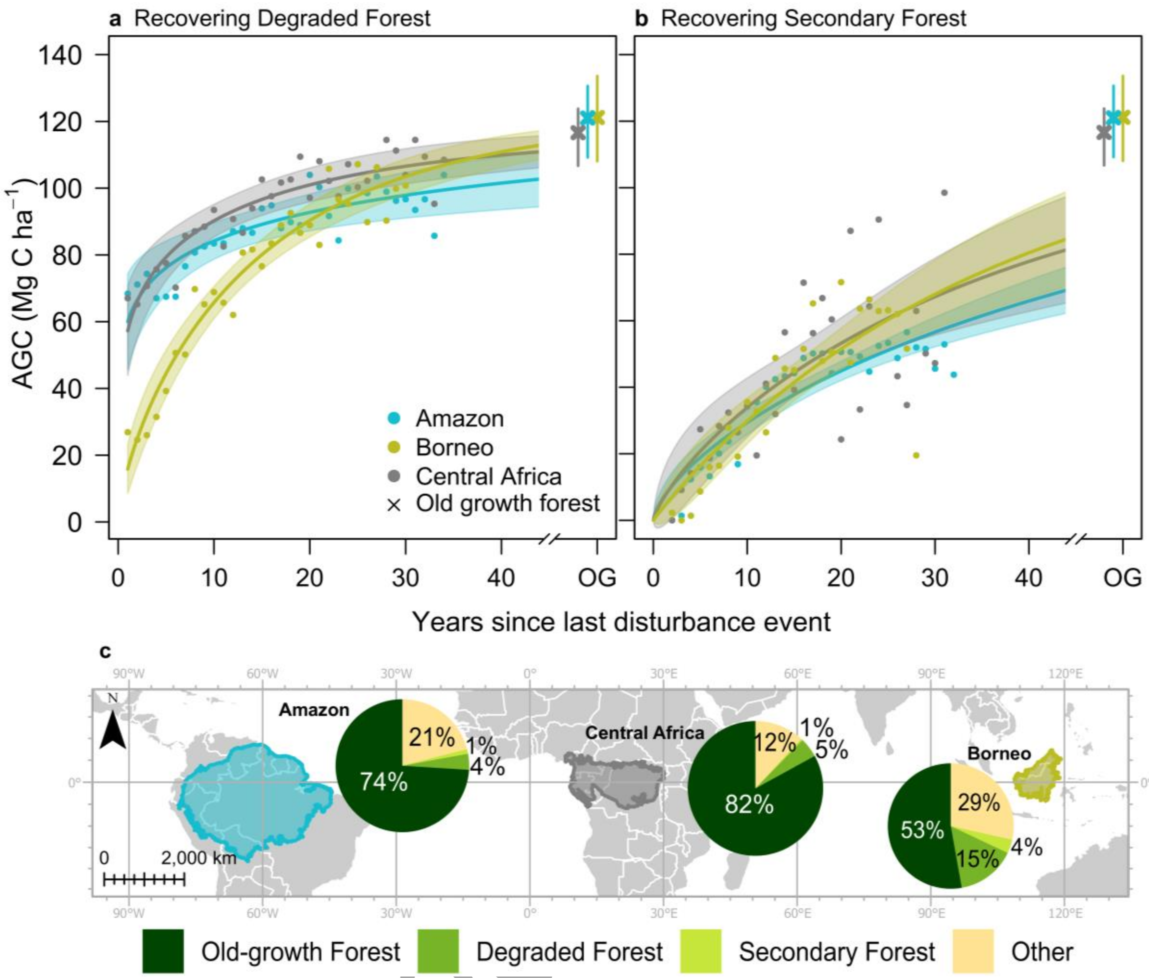

Figure 1 | Modelled Aboveground Carbon (AGC) accumulation with Years since last forest disturbance (YSLD) in different tropical regions. AGC is shown in (**a**) Degraded Forests and (**b**) Secondary Forests in the Amazon, Island of Borneo, and Central Africa tropical humid forest regions. Points denote the median AGC value calculated for each YSLD, fitted lines are based on a non-linear model (see methods). Shading denotes the 95% confidence interval of the non-linear model (Supplementary Discussion 1 for further exploration of variability and uncertainty). Crosses denote the median AGC of old growth (OG) forests in the respective regions and associated 95% confidence interval from the Monte Carlo simulation. (**c**) Map delineating the spatial extent used in this study representing each region as well as highlighting the percentage area occupied by different forest types used in this study as well as Other Lands. Map created using ESRI's ArcGIS Pro (2.6.0).

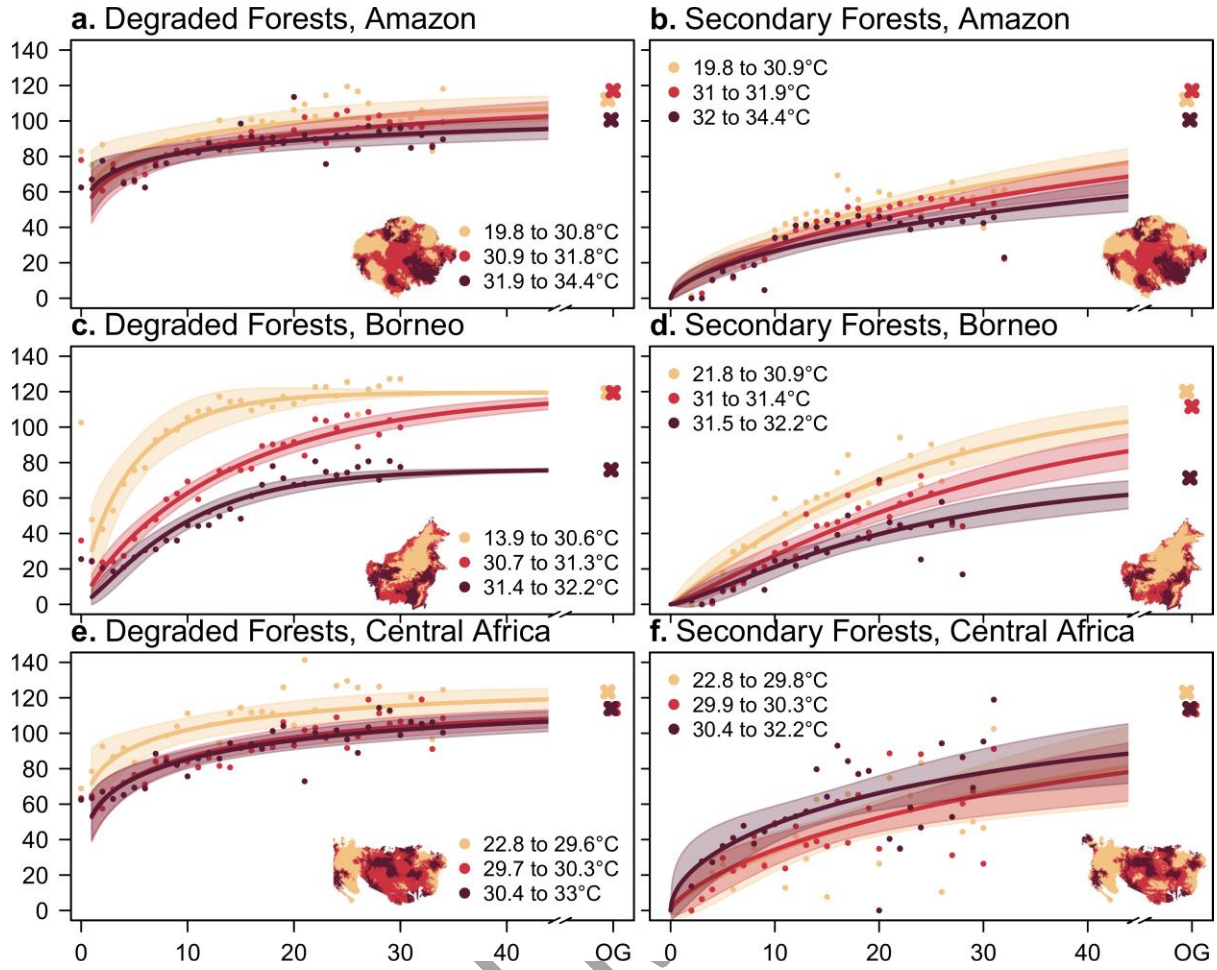

Figure 2 | Modelled Aboveground Carbon (AGC) accumulation in different maximum Temperature (Tmax) zones within different tropical regions. AGC as a function of Year since last disturbance event (YSLD) is shown for (a – b) the Amazon; (c – d) Borneo; and (e – f) Central Africa for Degraded Forests (left column) and Secondary Forests (right column). Points denote the median AGC value calculated for each YSLD, fitted lines are based on a non-linear model (see methods). Values in the legend denote the absolute lower 25% (yellow), middle 50% (red) and upper 25% (dark red) limits of the Tmax range in each location, which has units °C. Shading denotes the 95% confidence interval of the non-linear model. Crosses denote the median AGC of old-growth (OG) forests in the respective regions within the respective ranges of the variable. Each subplot contains a not-to-scale map of the region showing where the ranges for the Tmax bins can be found geographically. Maps were created using ESRI's ArcGIS Pro (2.6.0).

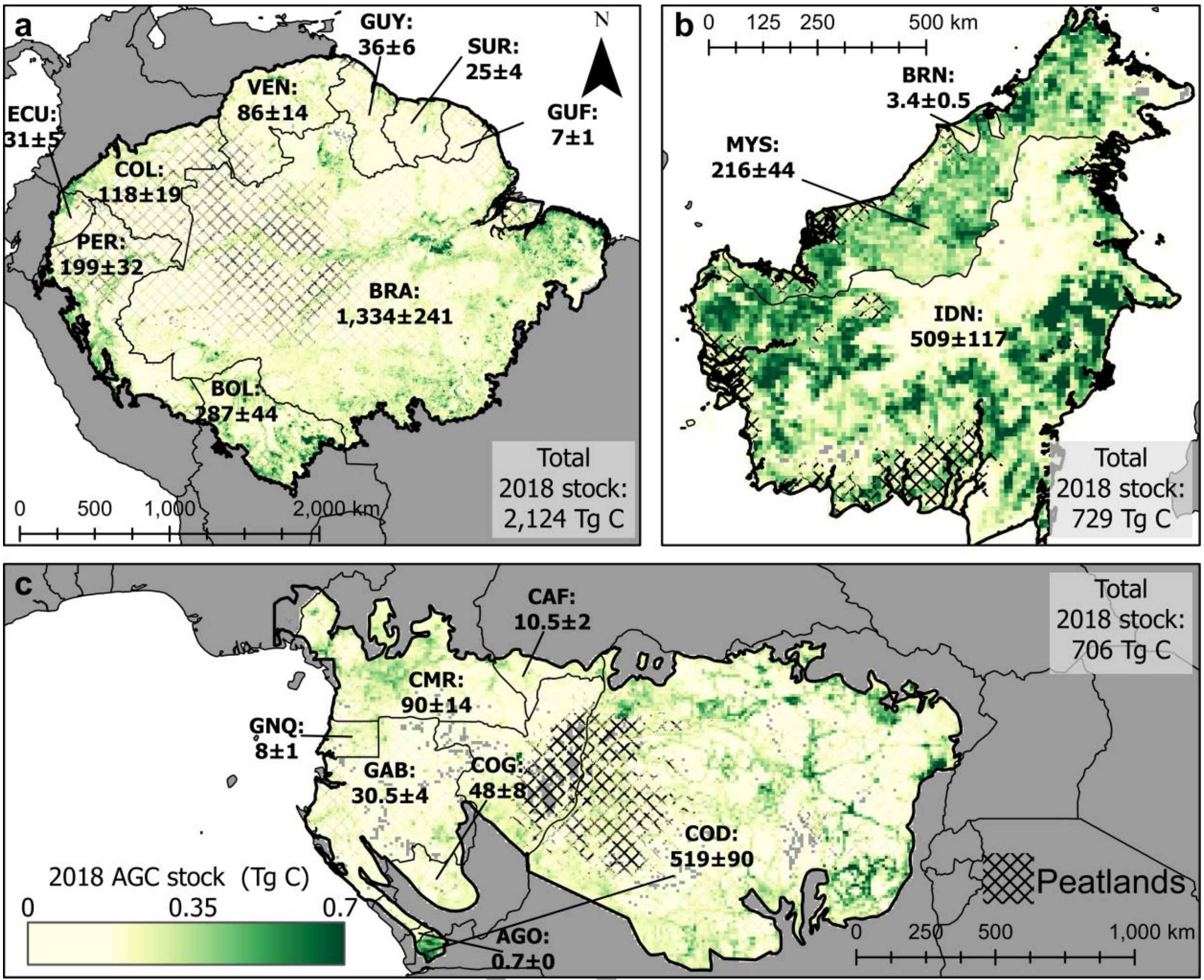

Figure 3 | The modelled 2018 carbon stock in recovering forests (degraded and secondary forests) within the three major tropical forest regions. The carbon stock shows the total carbon that has accumulated since the last disturbance event using the region-wide regrowth models developed in this study for (a) the Amazon, (b) Island of Borneo, (c) Central Africa Values of the carbon stock (Tg C) are aggregated to 0.1-degree grid squares and show the sum of degraded forest (Extended Data Figure 6) and secondary forest (Extended Data Figure 7), together representing recovering forest. Regions of peatland have been highlighted (see methods) and are denoted by the hatching. Annotated values denote the AGC stock and associated 95% confidence interval as estimated in this study using the Monte Carlo simulations per country expressed using ISO3 code for each country. Map created using ESRI's ArcGIS Pro (2.6.0).

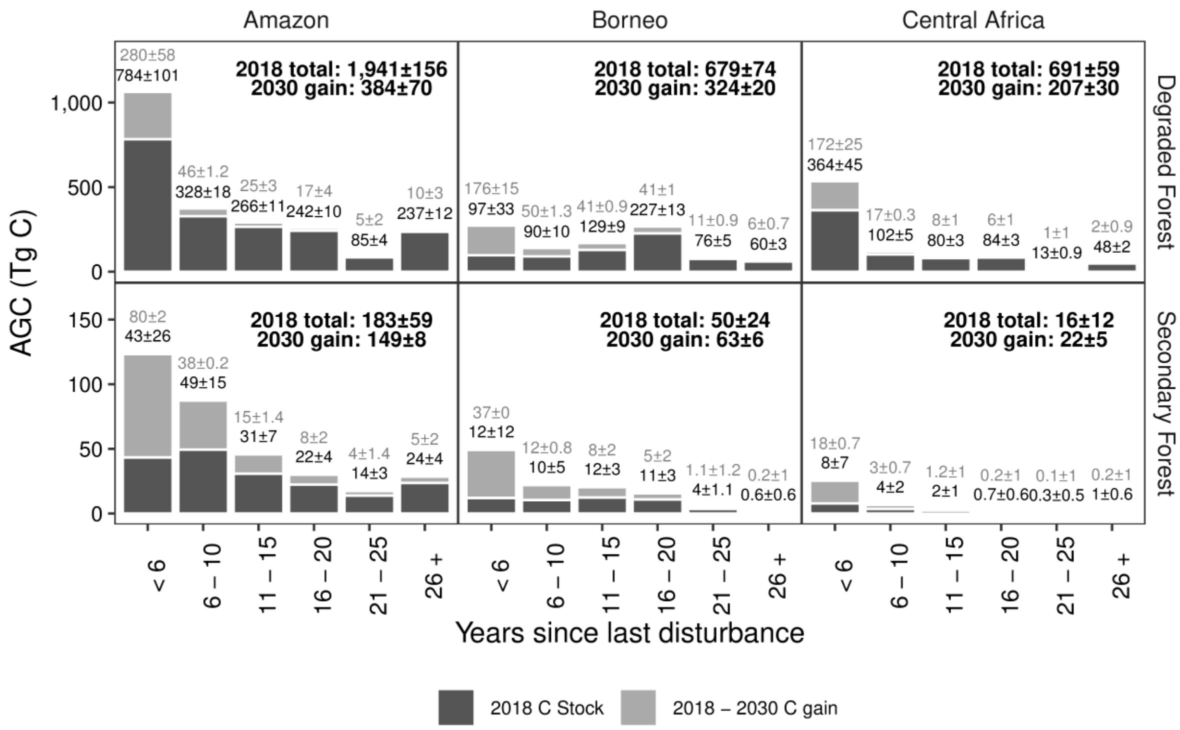

Figure 4 | The 2018 carbon stock and maximum technical 2030 carbon (C) sink potential across recovering forests within the three major tropical forest regions. Panels are split up according to the years since the forest was last disturbed and then further separated by region (columns) and forest type (rows). Solid bars denote the total carbon accumulated from the beginning of the growth period (since 1984 in Amazon and Central Africa, and since 1987 in Borneo) to 2018. Lighter bars denote the maximum potential carbon gain from 2018 to 2030 if the 2018 recovering forest area would remain until 2030. Black values refer to the 2018 carbon stock, grey values to the 2018 – 2030 maximum technical C gain. The range (±) shows the 95% confidence interval from the Monte Carlo simulations.

Extended Data Legends

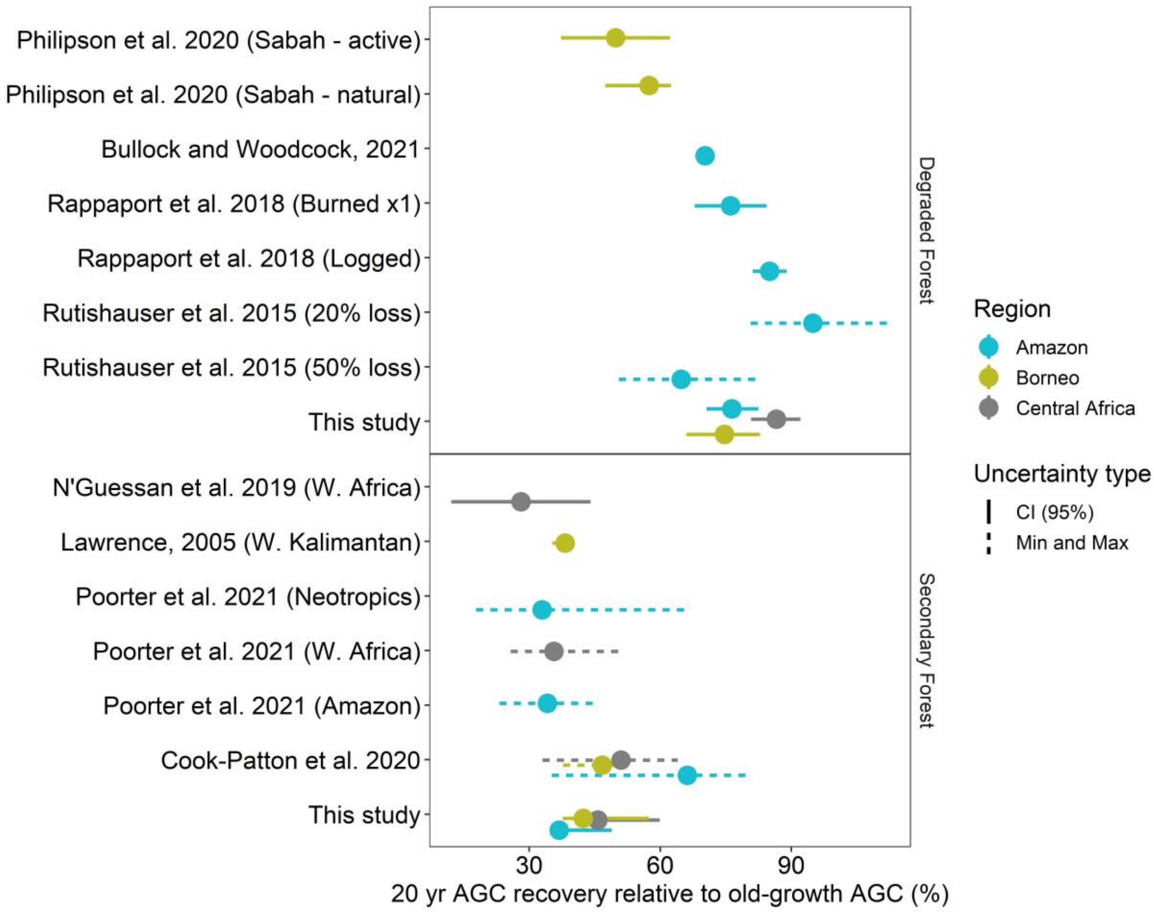

Extended Data Figure 1 | The Aboveground Carbon (AGC) after 20 years in recovering forests relative to old-growth forest values across different studies compared to this study. Values are expressed as the percentage (%) AGC recovered relative to old-growth forest values across the three study regions: Amazon, Borneo, and Central Africa in recovering degraded and secondary forests. Where previous studies capture a different region to those used in this study, the specific region has been indicated alongside the study name in brackets. E.g., W. Africa refers to West Africa in Poorter et al. and N'Guessan et al., this region is not in Central Africa but represents the closest region that could be found containing such information. Uncertainty types are either the 95% confidence interval (CI 95%) or the minimum and maximum values presented by the studies for the respective regions. More information on the previous studies and the associated values is given in the source data for this figure and the supplementary material.

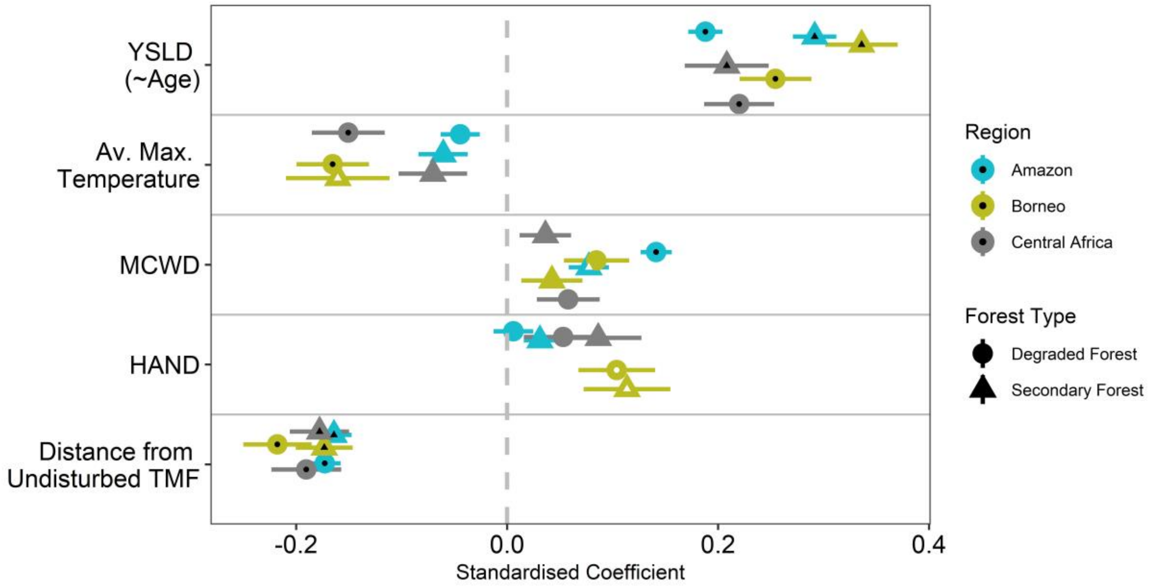

Extended Data Figure 2 | Correlation coefficients of different variables driving tropical Aboveground Carbon (AGC) (Mg C ha^{-1}). Values shown are the average standardised (to be within -1 and 1) coefficients from multiple general linear model runs based on spatial data that was sampled via stratified random sample accounting for spatial autocorrelation of the variables. The number of model runs to determine the average was based on the number of samples in each run such that the total sample size was 100,000. Bars denote the average standard deviation. Each coloured circle/triangle represents the respective standardised coefficient in degraded/secondary forests within the 3 regions (colours). Smaller shapes within the large, coloured shapes represent whether the result was statistically significant, where black denotes $p < 0.05$, white denotes $p < 0.1$ and no colour denotes $p >= 0.1$. The variables are Years since last Disturbance (YSLD) equivalent to age for secondary forests; Average Annual Maximum Temperature; Maximum Cumulative Water Deficit (MCWD); Height Above Nearest Drainage (HAND) and Distance from nearest undisturbed (old-growth) Tropical Moist Forest (TMF). The effects of MCWD are positive because the MCWD values are negative and so have an opposite effect: less negative values indicate less water deficit, which is associated with generally higher AGC and thus a positive coefficient.

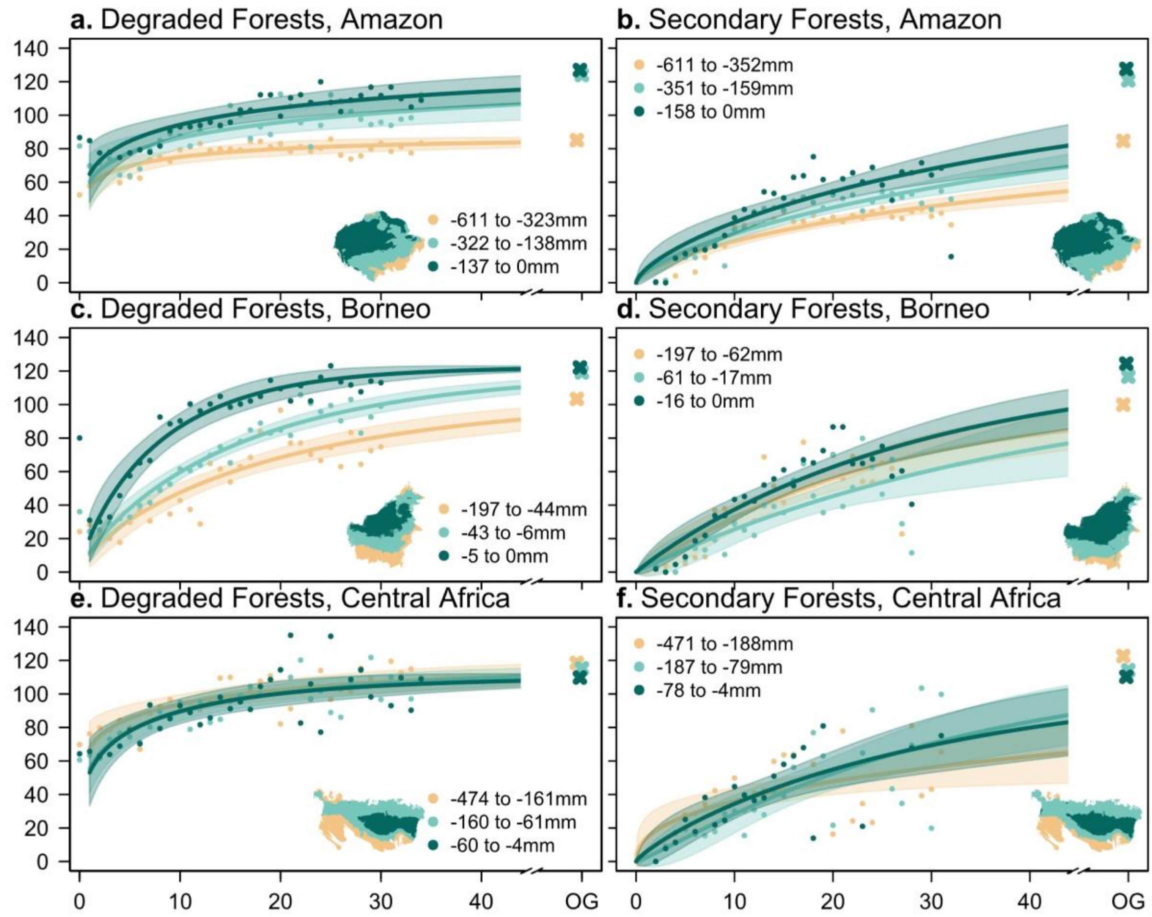

Extended Data Figure 3 | Modelled Aboveground Carbon (AGC) accumulation with Maximum Cumulative Water Deficit (MCWD) within different tropical regions. AGC as a function of Year since last disturbance event (YSLD) is shown in (a – b) Amazon; (c – d) Borneo; and (e – f) Central Africa for Degraded Forests (left column) and Secondary Forests (right column). Points denote the median AGC value calculated for each YSLD, fitted lines are based on a non-linear model (see methods). Values in the legend denote the absolute lower 25% (yellow), middle 50% (light green) and upper 25% (dark green) of the MCWD range, which has units -mm yr^{-1}. Shading denotes the 95% confidence interval of the non-linear model. Crosses denote the median AGC of old-growth (OG) forests in the respective regions within the respective ranges of the variable. Each subplot contains a not-to-scale map of the region showing where the ranges for the MCWD bins can be found geographically.

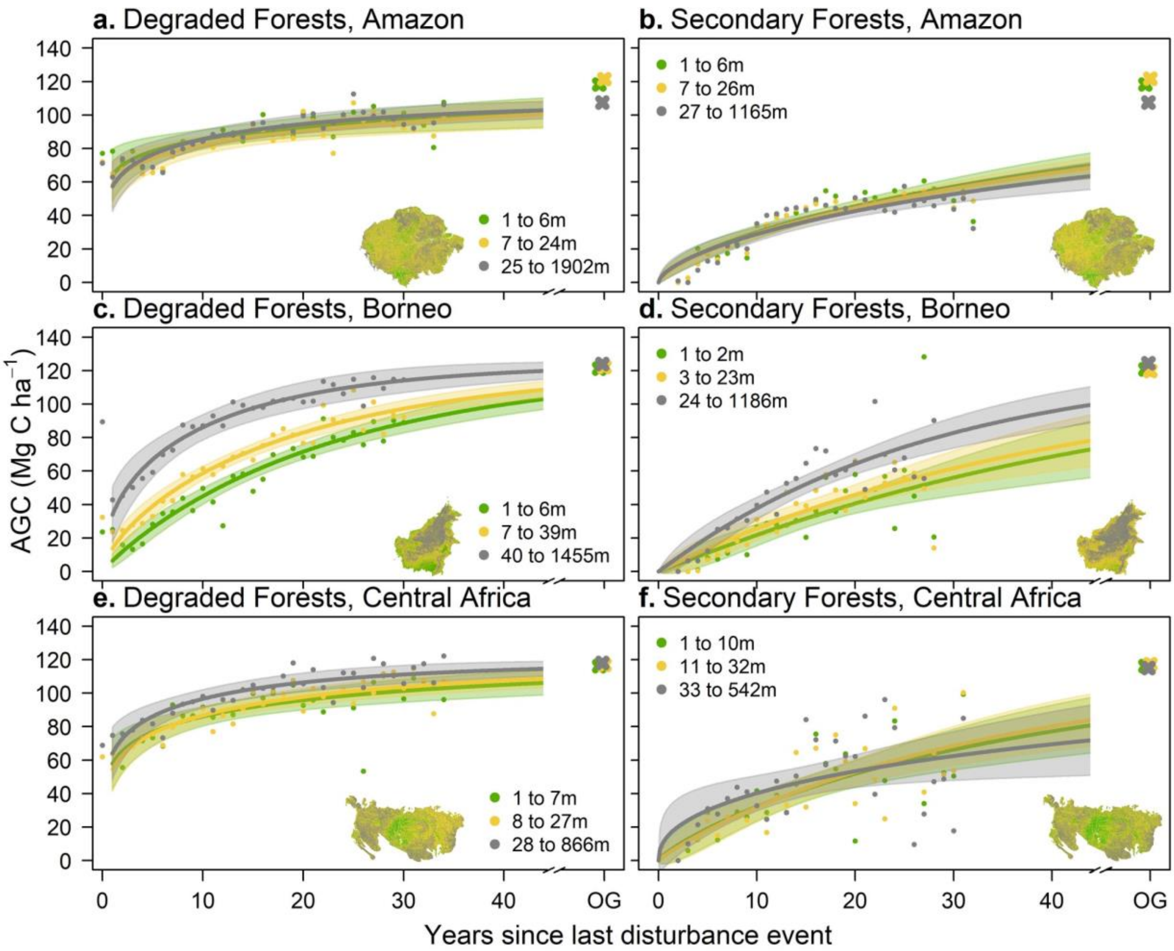

Extended Data Figure 4 | Modelled Aboveground Carbon (AGC) accumulation with Height Above Nearest Drainage (HAND) within different tropical regions. AGC as a function of Year since last disturbance event (YSLD) is shown in (a – b) Amazon; (c – d) Borneo; and (e – f) Central Africa for Degraded Forests (left column) and Secondary Forests (right column). Points denote the median AGC value calculated for each YSLD, fitted lines are based on a non-linear model (see methods). Values in the legend denote the absolute lower 25% (green), middle 50% (yellow) and upper 25% (grey) of the HAND range, which has units metres (m). Shading denotes the 95% confidence interval of the non-linear model. Crosses denote the median AGC of old-growth (OG) forests in the respective regions within the respective ranges of the variable. Each subplot contains a not-to-scale map of the region showing where the ranges for the HAND bins can be found geographically.

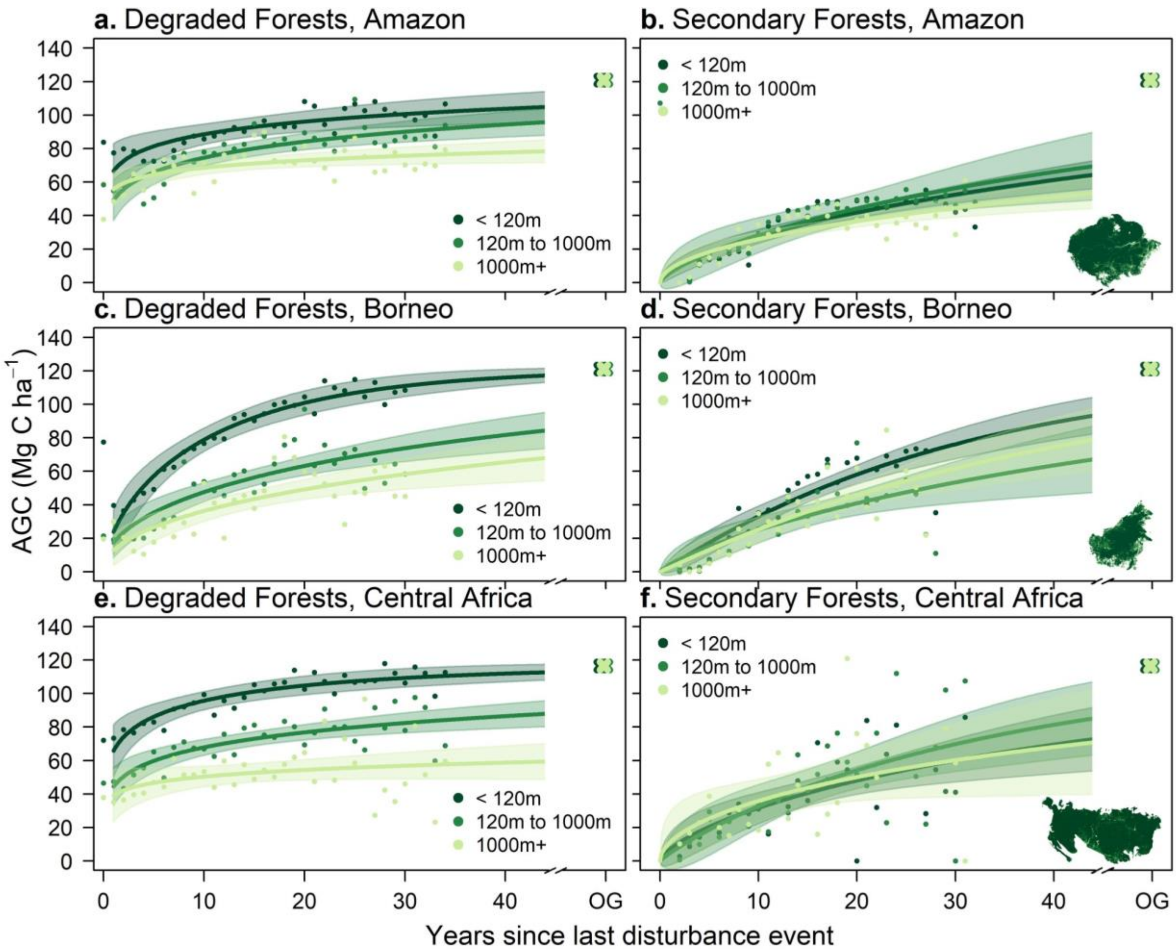

Extended Data Figure 5 | Modelled Aboveground Carbon (AGC) accumulation with distance from nearest old-growth forest within different tropical regions. AGC as a function of Year since last disturbance event (YSLD) is shown in (a – b) Amazon; (c – d) Borneo; and (e – f) Central Africa for Degraded Forests (left column) and Secondary Forests (right column). Points denote the median AGC value calculated for each YSLD, fitted lines are based on a non-linear model (see methods). Values in the legend denote the distances <120 m (lime green), 120m to 1000m (green) and 1000m + (dark green), representing the distance from the nearest old-growth forest. Shading denotes the 95% confidence interval of the non-linear model. Crosses denote the median AGC of old-growth (OG) forests in the respective regions within the respective ranges of the variable. In this case, only a single value of old-growth forest AGC is shown. Each subplot contains a not-to-scale map of the region showing where the ranges for the distance bins can be found geographically.

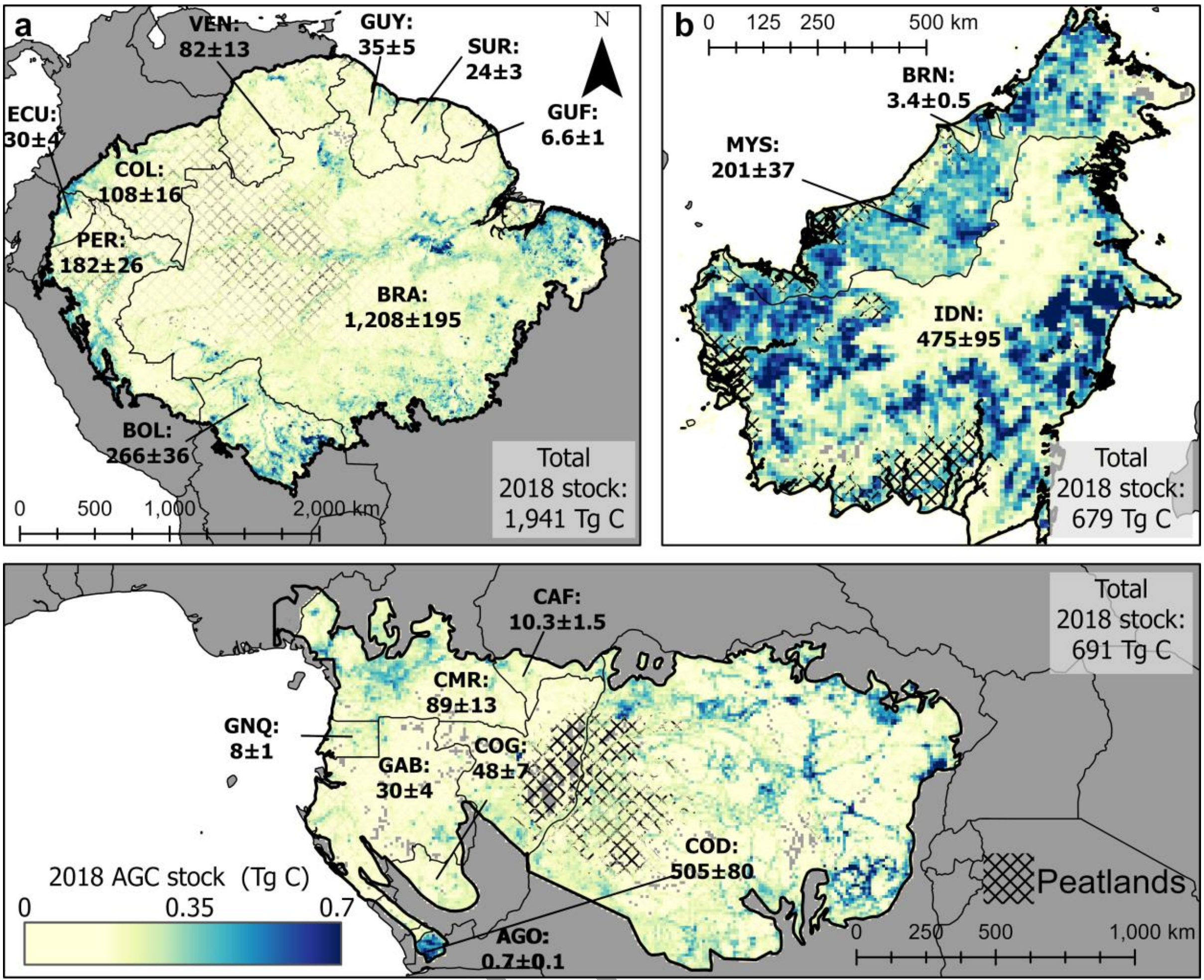

Extended Data Figure 6 | The modelled 2018 carbon stock in degraded forests within the three major tropical forest regions. The carbon stock shows the total carbon that has accumulated since the last disturbance event using the region-wide regrowth models developed in this study for (a) Amazon, (b) Island of Borneo, (c) Central Africa. Values of the carbon stock (Tg C) are aggregated to 0.1-degree grid squares and show the sum of degraded forest . Regions of peatland have been highlighted (see methods) and are denoted by the hatching. Annotated values denote the AGC stock and associated 95% confidence interval as estimated in this study using the Monte Carlo simulations per country expressed using ISO3 code for each country. Map created using ESRI's ArcGIS Pro (2.6.0).

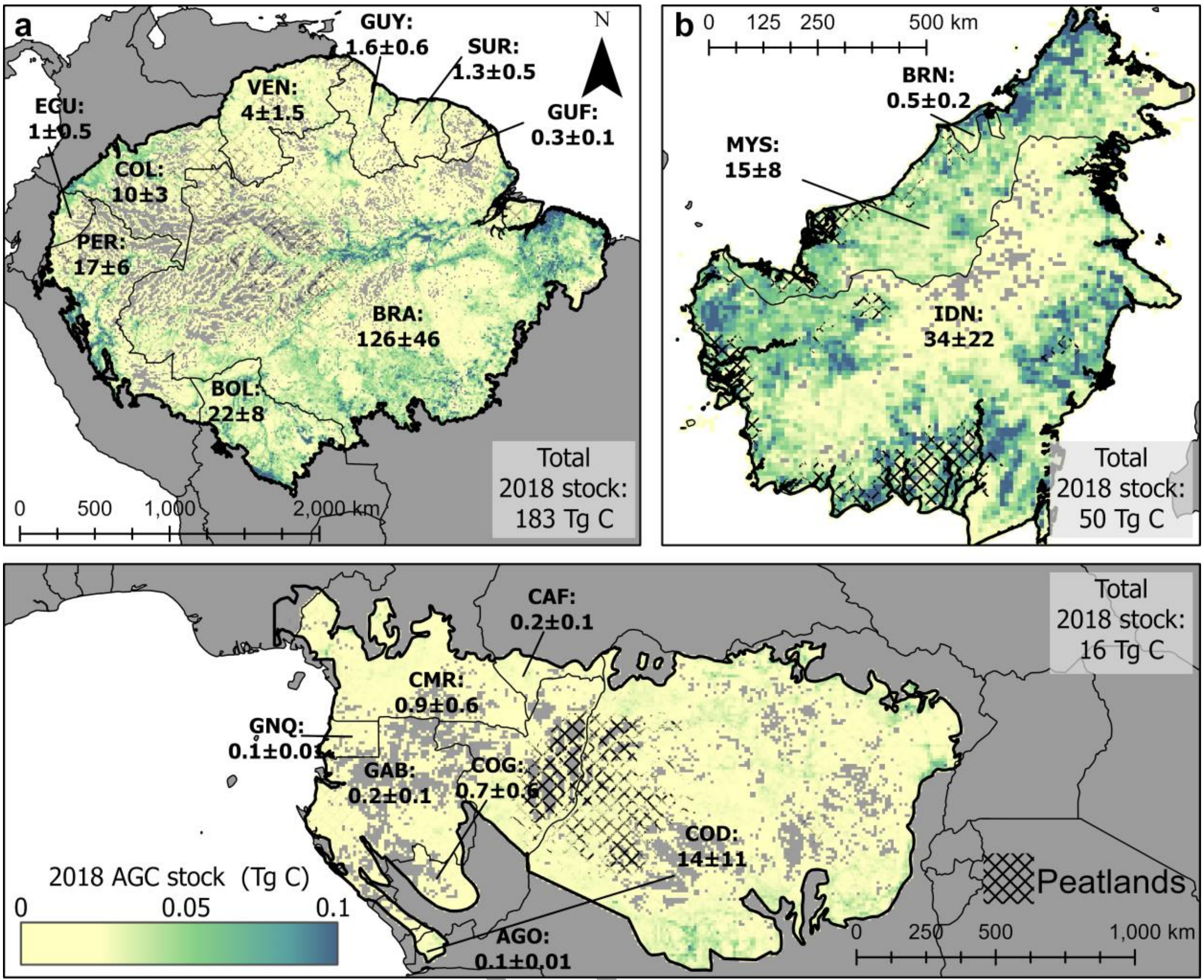

Extended Data Figure 7 | The modelled 2018 carbon stock in secondary forests within the three major tropical forest regions. The carbon stock shows the total carbon that has accumulated since the last disturbance event using the region-wide regrowth models developed in this study for(a) Amazon, (b) Island of Borneo, (c) Central Africa. Values of the carbon stock (Tg C) are aggregated to 0.1-degree grid squares and show the sum of secondary forest. Regions of peatland have been highlighted (see methods) and are denoted by the hatching. Annotated values denote the AGC stock and associated 95% confidence interval as estimated in this study using the Monte Carlo simulations per country expressed using ISO3 code for each country. Map created using ESRI's ArcGIS Pro (2.6.0).

Region	Total carbon emissions from: (Tg C)		Average forest area per year (1990 to 2018) lost due to (%):		Recovering forests (degraded + secondary forest)	
	Deforestation (From old-growth and degraded forest deforestation)	Degradation	Deforestation	Degradation	Total carbon removed (Tg C)	Contribution to counterbalancing forest loss emissions
Amazon	7,641 (7,596 to 7,740)	1,356 (965 to 1,746)	64%	36%	2,124 (1,808 to 2,541)	24% (19% to 30%)
Borneo	1,932 (1,905 to 1,960)	1,102 (886 to 1,261)	50%	50%	729 (589 to 913)	24% (18% to 33%)
Central Africa	948 (940 to 955)	458 (306 to 595)	29%	71%	707 (597 to 836)	50% (39% to 67%)
TOTAL	**10,521** **(10,441 to 10,655)**	**2,916** **(2,157 to 3,602)**	**57%**	**43%**	**3,560** **(2,994 to 4,290)**	**26%** **(21% to 34%)**

Extended Data Table 1 | Carbon emissions from forest loss and removals from recovering forest and their contribution to counterbalancing forest loss emissions accumulated up to 2018 across the three regions. Values refer to the sum of emissions/removals of Aboveground Carbon (AGC) in units Terragrams of carbon (Tg C) accumulated throughout the growth period (1984 to 2018). The emissions from deforestation were estimated based on the median value of old-growth forest AGC for each region, with the assumption that all AGC value was lost. Emissions from degradation were estimated by calculating the difference in AGC between old-growth forests and the first year since the last disturbance event. The emissions from deforestation included old-growth and degraded forest that were later deforested. Emissions from degradation only considered the AGC that was lost in degraded forests but later recovered. Values in brackets are the lower and upper estimates representing the 95% confidence interval from the Monte Carlo simulations.

Region	Percentage of degraded forests that were deforested by 2018	Total carbon emissions from degradation only (Tg C)	Total carbon removal potential from deforested degraded forest (Tg C)	Potential contribution to counterbalancing gross forest loss emissions (recovering + deforested-degraded forests) / (old-growth deforestation + observed degradation + potential degradation)
Amazon	37%	997 (710 to 1284)	1472 (1348 to 1603)	44% (34% to 51%) Mid: (2,124 + 1,472) / (5,732 + 1,472 + 997) Low: (1,808 + 1,348) / (5,811 + 1,746 + 1,603) Upper: (2,541 + 1,603) / (5,699 + 1,746 + 710)
Borneo	31%	552 (444 to 632)	440 (384 to 495)	39% (30% to 54%) Mid: (729 + 440) / (1,320 + 1,102 + 552) Low: (589 + 384) / (1,339 + 1,261 + 632) Upper: (913 + 495) / (1,301 + 886 + 444)
Central Africa	31%	270 (181 to 351)	420 (388 to 454)	96% (70% to 139%) Mid: (707 + 420) / (446 + 458 + 270) Low: (597 + 384) / (449 + 595 + 351) Upper: (836 + 454) / (441 + 306 + 181)
TOTAL	**35%**	**1,819** **(1,335 to 2,267)**	**2,332** **(2120 to 2,552)**	**48% (37% to 58%)**

Extended Data Table 2 | Percentage area of degraded forest that were deforested by 2018 and their potential carbon contribution to counterbalancing gross emissions from forest loss. The percentage area was calculated based on the total number of forest areas that had at one point (between 1984 and 2018) been classed as a degraded forest and the number of these areas that were deforested by 2018. The carbon removal potential was calculated based on the growth models for degraded forests in each of the three regions (Figure 1). Values in brackets are the lower and upper estimates representing the 95% confidence interval (CI) from the Monte Carlo simulations.

[End of manuscript]